國立交通大學

顯示科技研究所

碩士論文

Optimization of Hydrogenated Amorphous Silicon Single-Junction Solar Cells

氫化非晶矽薄膜太陽能電池之最佳化研究

研究生: 陳達欣　　　　Da-Shin Chen

指導教授: 蔡娟娟 教授　　Prof. C.C. Tsai

中華民國九十八年八月

氫化非晶矽薄膜太陽能電池之最佳化研究

Optimization of Hydrogenated Amorphous Silicon Single-Junction Solar Cells

研究生 ： 陳達欣　　　　Student: Da-Shin Chen

指導教授 ： 蔡娟娟 教授　　Advisor: Prof. C.C. Tsai

國立交通大學

顯示科技研究所

碩士論文

A thesis

Submitted to Department of Photonics

Display Institute

College of Electrical Engineering and Computer Science

National Chiao Tung University

In partial Fulfillment of the Requirements

For the Degree of

Master

In

Electro-Optical Engineering

August 2009

Hsinchu, Taiwan, Republic of China

中華民國九十八年八月

中文摘要

在此本論文中，我們利用射頻電漿輔助化學氣相沉積系統(RF-PECVD)在玻璃上沉積非晶矽薄膜太陽能電池。首先，對於本質非晶矽，p 型非晶矽跟 n 型非晶矽 的單膜的光電特性進行分析，並且找出最佳適用於薄膜太陽能電池。著我們利用加入甲烷 (CH$_4$)以改變 p 型非晶矽的光學特性，光學能隙可到 2 eV。但由於加入甲烷使得 p 型非晶矽的導電性變差，以必須選擇適當的條件。驗結果顯示太陽能電池加入非晶矽碳可以增加開路電壓從 0.75V 增加到 0.78V 短路電流也可以從 10.23mA/cm^2 到 12.76mA/cm^2。

一方面將太陽能退火處理，可使太陽能電池的特性變好。最佳的薄膜太陽能特性是效率是 8.67%。

Abstract

In this study, hydrogenated amorphous silicon (s-Si:H) solar cell was fabricated by plasma enhanced chemical vapor deposition (PECVD). First, we optimized condition of the deposited single layer for p-layer, i-layer and n-layer, respectively. In order to investigate film property, the optoelectronic and optical properties was measured by Fourier Transform Infrared Spectroscopy (FTIR), UV/VIS/NIR spectrometers. The property of hydrogenated amorphous silicon carbide (a-SiC:H) p-layer was measured and discussed. Comparing the photovoltaic performances of the as grown solar cell with p-layer for a-Si:H and a-SiC:H ,respectively. By using wide bandgap p-layer, the open-circuit voltage (V_{oc}) increased from 0.75V to 0.78V with corresponding short-circuit current (J_{sc}) increased from 10.23mA/cm^2 to 12.76mA/cm^2. Post-treatment of the cell was also carried out and significant increase in the fill factor (FF), efficiency, and V_{oc} were observed. The experiment result showed an improvement between the Ag back electrode and amorphous n-layer. Different cell area of 2×2 cm^2 and 1×1 cm^2 were also fabricated. A cell conversion efficiency of 8.67% was achieved for a cell area of 2×2cm^2.

誌謝

Contents

Figure Captions

Table Captions

Chapter 1 Introduction

1.1 Preface

The world is currently dependent on fossil fuels and other sources of non-renewable energy. The constant consumption and world-wide demography expansion add to the potential risks of ecological and human disaster associated with global warming. These reserves are finite resources and as such the need to reduce our dependency on them is widely agreed on, to the point where ideally energy generation could be self sustaining over the whole planet. This makes it a necessity to develop renewable energy technologies. Renewable energy can be harvested from many natural sources including wind, geothermal heat, sunlight, hydroelectricity, etc. From the Figure1.1, the solar power has more potential to compensate energy gap.
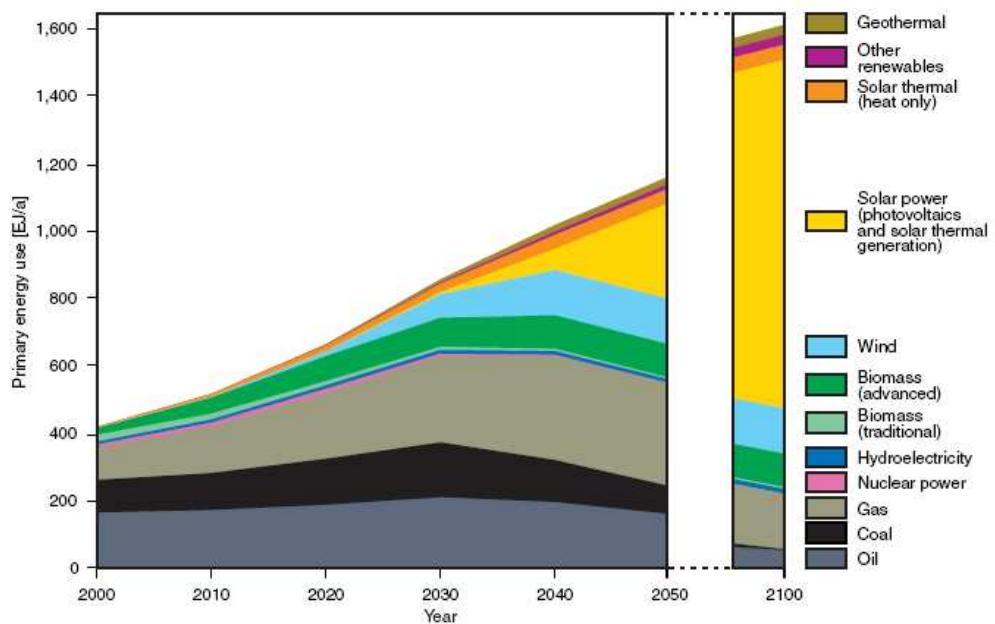
Figure 1.1 Transforming the global energy mix: The exemplary path until 2050/2100 [1]

Solar Cells are classified into three generations which indicates the order of which each became important as shown in Figure 1.2. First generation cells consist of wafer base, high quality and single-junction devices. But the cost is too high. Second generation cells is thin film solar cell such as a-Si:H solar cell ,CIGS, CdTe, etc. These materials are applied in a thin film to a supporting substrate such as glass reducing material mass and therefore costs. Third generation technologies aim to enhance poor electrical performance of second generation (thin-film technologies) while maintaining very low production costs. It involves new material and new solar cell structure. In this work, we will focus on second generation, amorphous silicon solar cell.
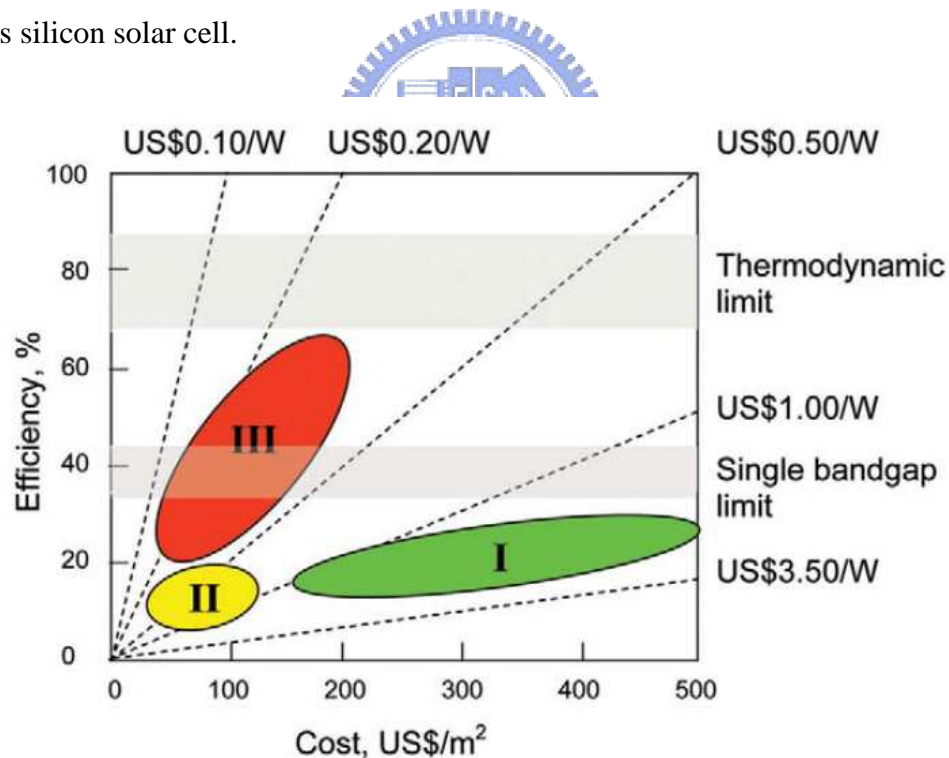
Figure 1.2 Efficiency and cost projections for first-, second- and third-generation PV technologies (wafer-based, thin films, and advanced materials and structures, respectively) [2]

1.2   Amorphous Silicon and Crystalline Silicon

Figure 1.3 illustrates the different silicon network in crystalline silicon and hydrogenated amorphous silicon. Crystalline silicon is a four-fold coordinated atom that is normally tetrahedrally bonded to four neighboring silicon atoms. The tetrahedral structure is continued over a large range, forming a well-ordered lattice (crystal), as shown in Figure 1.3 (a).

Hydrogenated amorphous silicon (a-Si:H) is the non-crystalline allotropic form of silicon. It can be deposited in thin films at low temperatures onto a variety of substrates. In amorphous silicon this long range order is not present and the atoms form a continuous random network, as shown in Figure 1.3 (b). Although amorphous silicon lacks the long range order, it has the same short range as single crystalline silicon. Due to the disordered nature of the amorphous silicon, some silicon atoms have a dangling bond. There are covalently bonded to only three silicon atoms and have on unpaired electron, a so-called dangling bond. These dangling bonds are defects in the silicon random network, which cause anomalous electrical behavior.
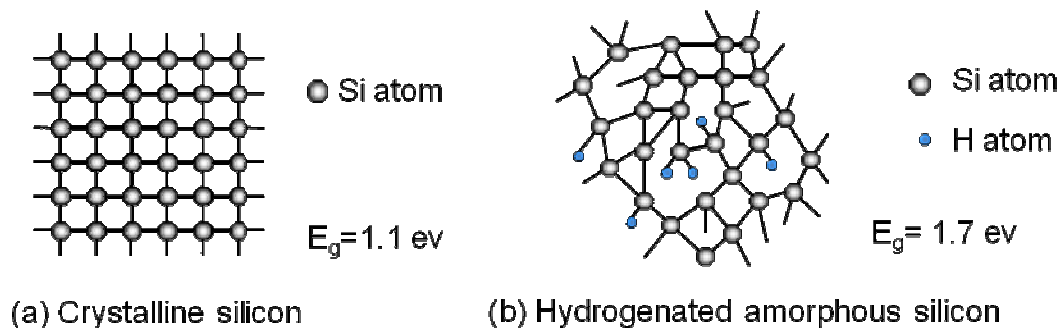
Figure 1.3   Silicon network in (a) crystalline silicon (b) hydrogenated amorphous silicon.

When amorphous silicon was deposited in such a way that hydrogen can be incorporated in the atomic network, the material can be passivated by hydrogen. Thus, the dangling bond density can reduce by several orders of magnitude. In general, there exist about 10 at.% hydrogen concentrations in hydrogenated amorphous silicon thin film. Because hydrogen radical would passivate dangling bond, hydrogenated amorphous silicon has a sufficiently low amount of defects to be used within devices. Due to Si-H bonding (1.7eV) was formed, amorphous silicon bandgap (1.75eV) is large than crystalline silicon bandgap (1.12eV). However, the hydrogen is unfortunately associated with light induced degradation of the material, termed the Staebler-Wronski effect.
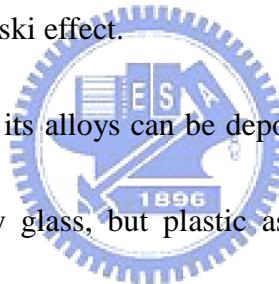
One advantage is that a-Si or its alloys can be deposited at very low temperatures. This allows for deposition on not only glass, but plastic as well, making it a candidate for a roll-to-roll processing technique [4-6]. Another advantage is that amorphous silicon can be deposited over large areas by PECVD.

1.3 The Structure of Thin Film Solar Cell

There are two basic configurations of thin film solar cell, as shown in Figure 1.4. From the Figure 1.4(a), it is termed superstrate configuration and the substrate usually is used transparent material. The p-layer is deposited first, then the intrinsic layer and the n-layer deposited last. From the Figure 1.4(b), it is substrate configuration and occurs when a cell is deposited onto an opaque substrate. The sequence of process reversed to the supertrate

configuration. In the case of the superstrate configuration, the glass usually was coated with transparent conductive oxide (TCO) film. In addition, the TCO layer has to be surface textured in order to enhance light absorption inside the solar cell due to the scattering at internal rough interface.
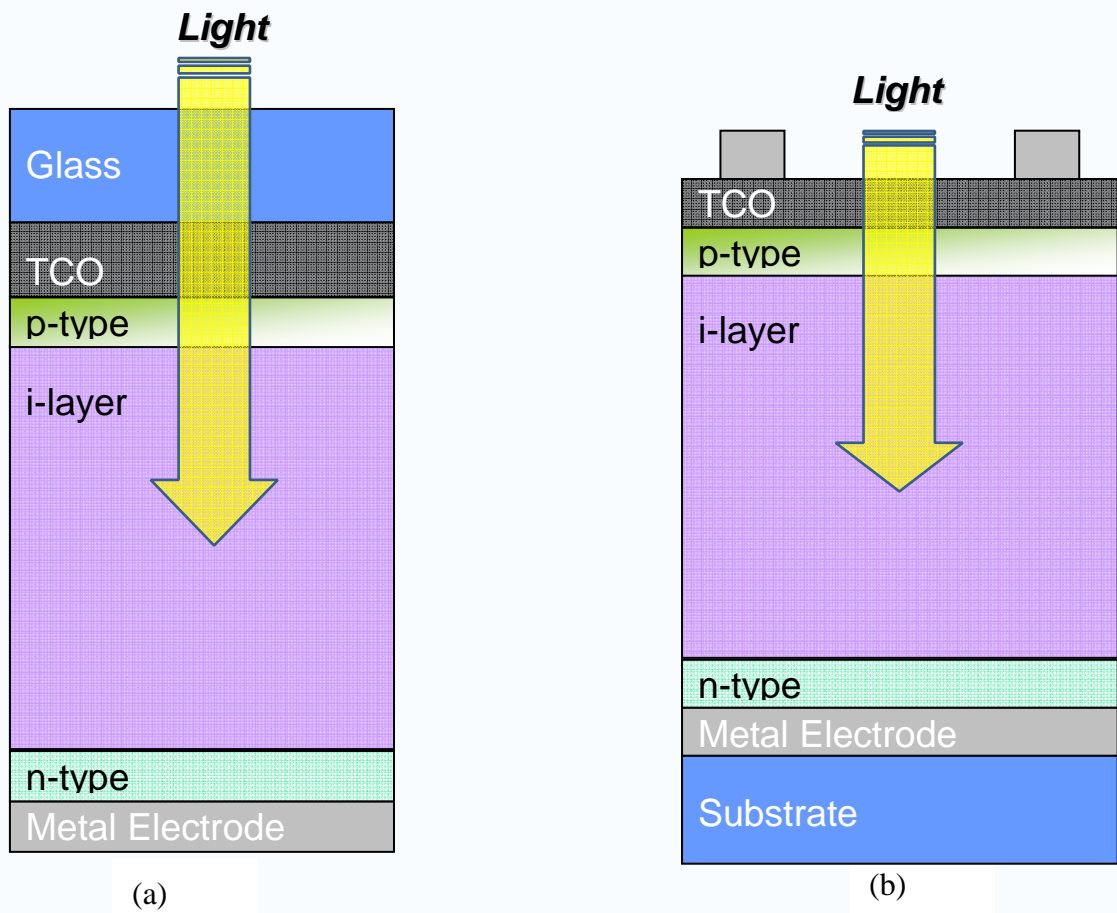
Figure 1.4   (a) The superstrate cell configuration and (b) the substrate cell configuration.

Thin film a-Si:H must be grown with an intrinsic region as opposed to pn junction to compensate for low carrier drift mobility. The electric field across the intrinsic region is required to achieve effective separation of generated carriers and a rectifying junction.

Both configurations are usually illuminated through a TCO/p-layer interface. This improves cell performance by generating most carriers close to this interface, lowing hole recombination probability. Due to the low hole mobility of a-Si:H, efficient collection is a priority for ensuring good cell performance. So the p-layer also call window layer in the solar cell structure.

1.4 AM1.5 Light Source

Solar radiation closely matches a black body radiator at 5,800 K. As the sunlight travels though the atmosphere, chemicals react with the sunlight and absorb certain wavelengths. Perhaps the best known example is the stripping of ultraviolet light by ozone in the upper atmosphere, which dramatically reduces the amount of short wavelength light reaching the Earth's surface. A more active component of this process is water vapor, which results in a wide variety of absorption bands at many wavelengths, while molecular nitrogen, oxygen and carbon dioxide add to this process.

Atmospheric scattering also plays a role, removing higher frequencies from direct sunlight and scattering it about the sky. The greater the distance of atmosphere the sunlight travels through, the greater this effect, which is why the sky looks pink at sundown when the sunlight is traveling obliquely through the atmosphere.

For a thickness l_o of the atmosphere, the path length l through the atmosphere for solar radiation incident at angle θ relative to the normal to the Earth's surface is

$$l = l_o / cos\ \theta \tag{1}$$

The ratio l / l_o is the air mass coefficient.

As shown in Figure 1.5, the spectrum outside the atmosphere, the 5,800 K black body, is referred to as "AM0", meaning "zero atmospheres". Cells used for space power applications, like those on communications satellites are generally characterized using AM0.
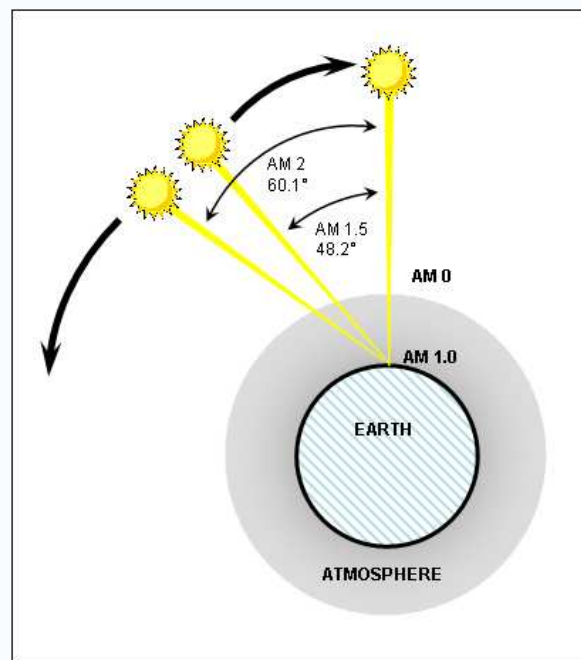
Figure 1.5   Schematic of air mass

The spectrum after traveling through the atmosphere to sea level with the sun directly overhead is referred to as "AM1". This means "one atmosphere". Conveniently, silicon solar cells are not very sensitive to the portions of the spectrum lost in the atmosphere. Since solar

7

cell development is concentrated in the United States, Europe and Japan, an AM number representing the spectrum at mid-latitudes is much more common. "AM1.5", which is 1.5 times the atmosphere thicknesses, corresponds to a solar zenith angle of 48°, and is almost universally used to characterize solar panels. "AM1.5G", where G stands for 'global' and includes both direct and diffuse radiation.

1.5 Staebler–Wronski Effect

The Staebler-Wronski Effect (SWE) refers to light-induced metastable changes in the properties of hydrogenated amorphous silicon. The defect density of hydrogenated amorphous silicon (a-Si:H) increases with light exposure, to cause an increase in the recombination current and lead to the reduction in the sunlight to electricity conversion efficiency. It was discovered by Staebler and Wronski in 1977 [3]. They showed that the photo-conductivity of hydrogenated amorphous silicon can be reduced significantly by prolonged illumination with intense light. However, it could reverse the effect by heating the samples to above 150℃.

The efficiency of an amorphous silicon solar cell typically drops during the first six months of operation. This drop may be in the range from 10% up to 30% depending on the material quality and device design. After this initial drop, the effect reaches equilibrium and causes little further degradation. Most commercially available a-Si modules have SWE degradation in the 10 to 15% range and suppliers typically specify efficiency based on performance after the SWE degradation has stabilized. In a typical amorphous silicon solar

cell the efficiency is reduced by up to 30% in the first 6 months as a result of the

Staebler–Wronski effect, and the fill factor falls from over 0.7 to about 0.6. This light induced

degradation is the major disadvantage of amorphous silicon as a photovoltaic material.

1.6 PECVD

Plasma enhanced chemical vapor deposition (PECVD) system is widely used to fabricate

silicon thin film solar cell. Using PECVD system to deposit silicon thin film is a low

temperature process, usually less than 300℃. So silicon thin film can deposit onto variety of

substrates such as glass, stainless steel, or plastic substrate. Comparing the silicon wafer

substrate, employing the above substrates is the good point of view to industry for large scale

productions and cost drop. Besides, doping and alloy layers are made easily by using PECVD

method. For example, introducing source gases SiH_4 and B_2H_6 or SiH_4 and PH_3 mixture,

doping layers can be easily deposited onto different substrates.
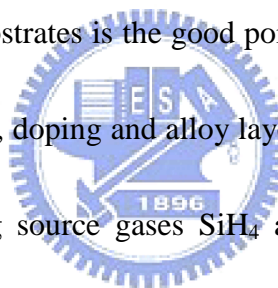
1.7 An Overview of Amorphous Silicon Solar Cell

First commercially available thin-film solar cells based on a-Si:H were produced for

consumer applications such as pocket calculators and solar watches. Today, a new generation

of a-Si:H-based solar modules enters the market focusing on power applications. Several

manufacturing facilities with multi-megawatt capacity have started production, are currently

being installed, or are announced [4, 7, 8].

The development of the first a-Si:H solar cell was reported by Carlson and Wronski

in 1976 [9]. This single junction p-i-n a-Si:H solar cell deposited on a glass substrate coated with transparent conductive oxide (TCO) and aluminium back contact exhibited a 2.4% conversion efficiency. Only one year later Staebler and Wronski discovered the light-induced degradation of a-Si:H (Staebler–Wronski effect, SWE) [3]– a severe drawback in a-Si:H solar cell technology. During exposure of solar cells to light the SWE results in a decrease of efficiency until a saturation value is reached. Since the recognition of the SWE, development strategies have focused on improvements of the stabilized efficiency reached after long-term operation. The stacked-cell concept has emerged as a powerful tool to enhance the stabilized efficiency [10]. Moreover, the use of component cells with different optical bandgaps provides a better utilisation of the solar spectrum [11, 12].
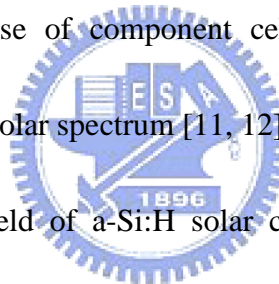
Much research in the field of a-Si:H solar cell was devoted to developing and optimizing a-Si:H base alloys in the 1980s. A p type hydrogenated amorphous silicon carbide (a-SiC:H) was incorporated in solar cells as a low absorbing layer, usually denoted as a window layer [13]. Hydrogenated amorphous silicon germianium (a-SiGe:H) became an attractive low bandgap material for stacked solar cells [14]. Surface textured substrates were introduced to enhance optical absorption [15]. Optimized transparent conductive oxide (TCO) films and TCO/metal back reflectors minimize reflection losses and provide an effective light trapping.

The application of high hydrogen dilutions during the growth of intrinsic a-Si:H and

a-SiGe:H (hydrogenated amorphous silicon germanium) films and corresponding alloys improves the electronic properties of these materials in both the initial and the light-soaked state [16–18]. All these techniques are combined in a triple-junction a-Si∕a-SiGe:H∕a-SiGe:H cell which yields a stable active area efficiency of 13% [12]. This value represents the current world record for solar cells based on a-Si:H and its alloys. Hydrogenated microcrystalline silicon deposited by the low temperature PECVD technique emerged in this period as a new candidate for the low bandgap material in multijunction a-Si:H based solar cells [19].

Research has concentrated on understanding and improving light trapping techniques, where surface textures as well as new TCO material play a crucial role. This activity has resulted in the commercialization of novel deposition techniques for ZnO as an alternative TCO material for SnO_2 [20]. Several deposition machine manufacturers have started developing commercial production machines for the fabrication of thin film silicon solar cell [21]. Most improvements in stabilized solar cell efficiency are based on adapted cell designs and advanced light-trapping concepts. Many fundamental questions remained regarding the growth and the material properties of a-Si:H and its alloys as well as the optical and electrical function of complete solar cell devices.

1.8 Motivation

Thin film silicon in general, are expected to be promising material for applications to optoelectronic device. Many growth methods have been proposed for the preparation of

device-grade a-Si:H, reactive sputtering, mercury-sensitized photo-chemical-vapor deposition (CVD), direct-photo CVD, hot-wire CVD, and plasma-enhanced CVD (PECVD). Among the variety of growth methods, PECVD is widely used due to its high potential for yielding a uniform high-quality silicon thin film on a large-area substrate.

In this study, hydrogenated amorphous silicon (s-Si:H) solar cell was fabricated by Radio-Frequency Plasma Enhanced Chemical Vapor Deposition (PECVD). The absorption in the a-Si:H intrinsic layer contributes to the current generation, the optimal optical and optoelectronic property was crucial role for solar cell performance. Due to lower mobility of holes in comparison to electrons in a-Si:H , the p-layer a-Si:H of quality is the other effect for solar cell performance. Because light enters the solar cell through the p-layer, there is substantial absorption in this layer. The photogenerated carriers in the p-layer do not contribute to the photocurrent because the electron quickly recombined. Therefore, the absorption of the p-layer has to minimize, which is done by minimizing the thickness and alloying the p-layer with carbon.

1.9 Thesis Outline

This thesis is organized into the following chapters:

In the chapter 1, a brief overview of thin film solar cell technology is introduced to describe its advantages and bottlenecks. The motivation of the studies is also described in chapter one.

In the chapter 2, the process flow of the samples is introduced. The measurement method also shows here in detail.

In the chapter 3, here shows the dependence of material properties and device performance on various conditions with different hydrogen dilution ratios.

In the chapter 4, this chapter will discuss the results from chapter 3. The effect and the dependence of the material properties on different conditions will be explain here.

In the chapter 5, the results of our experiments in chapter 3 and discussions in chapter 4 are concluded.

Chapter 2　　Experimental Details

2.1　Radio-Frequency Plasma-Enhanced Chemical Vapor Deposition

Plasma-enhanced chemical vapor deposition (PECVD) is common technique used during the manufacturing of most microeletronic device. The role of the plasma is to provide a source of energy to dissociate silicon bearing gas, which is usually silane (SiH_4), hydrogen (H_2), etc. This is done by collisions with electrons, which originate as secondary electrons in the plasma an build up their energy by acceleration in an electric field. The growth of an a-Si:H film is accomplished by attaching reactive particles of dissociated silane molecules, call radicals, to the surface of the growing film. It consists in the excitation of a gas, of a mix gases, by an electric field between two electrodes as sketched in Figure 2.1.
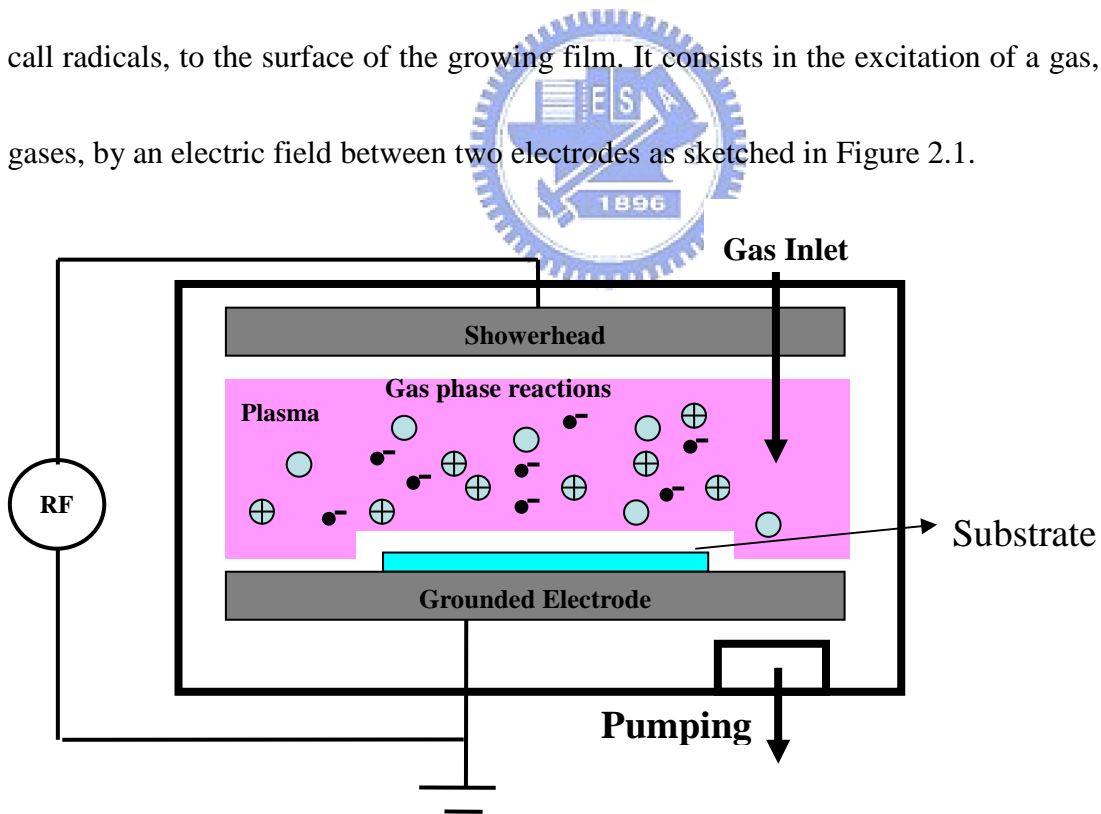
Figure 2.1　　Schematic diagram of capacitively-coupled rf PECVD system

The initial event in the growth process of a-Si:H is electron-impact dissociation of the source gas materials in silane (SiH_4) and silane-to-hydrogen (SiH_4/H_2) glow-discharge plasma. SiH_4 and H_2 molecules were through electronic excited states of these molecules by inelastic collisions with high-energy electros in the plasma. Electronic excited states of complicated molecules such as SiH_4 are usually dissociating states at which dissociation occurs spontaneously to SiH_3, SiH_2, SiH, Si, H_2 and H.

Reactive neutral and ionic species produced in the plasma undergo secondary reaction mostly with SiH_4 and H_2 molecules, forming a steady state. Rate constants for each reaction are summarized in the literature [22]. Therefore, highly reactive species such as SiH_2, SiH, and Si (short-lifetime species) have much smaller values of densities than SiH_3 in the steady-state plasma, although the generation rates of those species are not very different from that of SiH_3, which indicates low reactivity with SiH_4 and H_2(long-lifetime species).

In the growing amorphous silicon, the SiH_3 radicals reaching the film-growing surface start to diffuse on the surface. During surface diffusion, SiH_3 abstracts surface-covering bonded hydrogen, forming SiH_4 and leaving a dangling bond on the surface (growth-site formation). Another SiH_3 radical toward the dangling-bond site on the surface and forms the Si-Si bond (film growth), as schematically shown in Figure 2.2. This surface reaction scheme for film growth has been proposed on the basis of two experimental results [23].
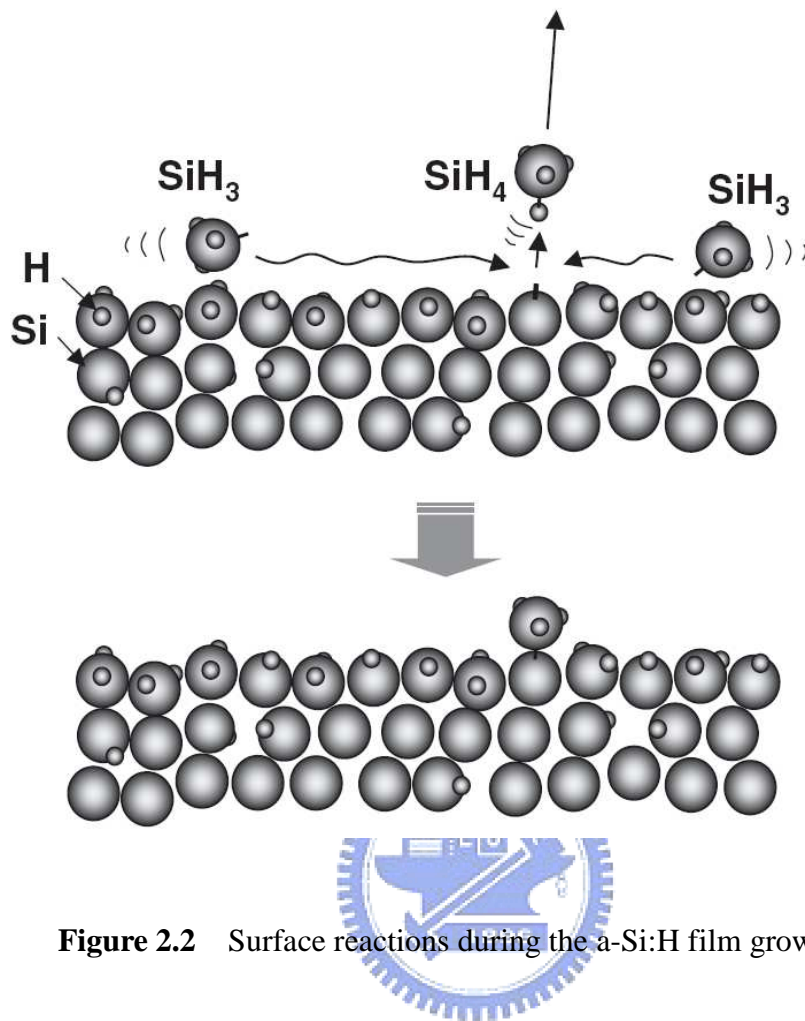
Figure 2.2   Surface reactions during the a-Si:H film growth [23]

Through other radicals contribute much less to the growth, they do play an important role in determining the properties of the film. The SiH_2 and higher silane radicals have higher sticking coefficients than SiH_3 and be incorporated directly into the hydrogen terminated surface [24]. However, the contribution of these radical to the growth results in poor quality film, and therefore the presence of these radicals in the plasma should to be avoided.

An important advantage of plasma enhanced CVD deposition is that the deposition is that the deposition temperature of device quality a-Si:H is usually between $200℃$ and $250℃$.

2.2 Introduction of Experiment

Hydrogenated amorphous silicon films were deposited using pure SiH_4 by radio frequency (27.12 MHz) plasma enhanced chemical vapor deposition (PECVD) system. Doping layers were prepared by using B_2H_6 or PH_3 with pure SiH_4 and H_2 dilution. Amorphous silicon carbide was deposited by mixing SiH_4 and CH_4. Prior to deposit all the samples, the chamber was introduced gas NF_3 and Ar to clean the chamber. Corning Eagle2000 glass and crystalline silicon wafer substrate were clean by KG Cleaner and RCA standard cleaning process, respectively. All the samples were started to prepare after the background pressure of the reactor chamber reach to 10^{-7} torr. In this study, samples were prepared simultaneously on 5.0 cm * 5.0 cm Corning Eagle 2000 glass and 1.5cm * 1.5cm c-si wafer. The samples gown on glass substrate was used to analysis optoelectrial properties and the films on c-si wafer were used to determine the hydrogen bonding configuration. The devices were deposited on the glass coated TCO.

The complete range of deposition conditions include: substrate temperature (T_S) : 190~210°C, pressure: 0.3~1 torr, background pressure: 10^{-7} torr, power: 20~40 W, electrode spacing (E/S): 13-25 mm.

2.3 Determination of Thin Film Thickness

The measurement of thin film thickness has a lot of methods such a Alpha stepper and ellipsometery. In the measurement of the alpha stepper, it has to be step profile. So chemical etching is necessary to make step high. Chemical etching may occur by any of several different processes. The simplest modes of etching involve dissolution of the material in a liquid solvent without any change in the chemical nature of the dissolved species. So choosing solvent is important for chemical etching. And we find the material, 30 wt.% KOH, can etch silicon. Although it still etches silicon dioxide, it etches slowly at room temperature.
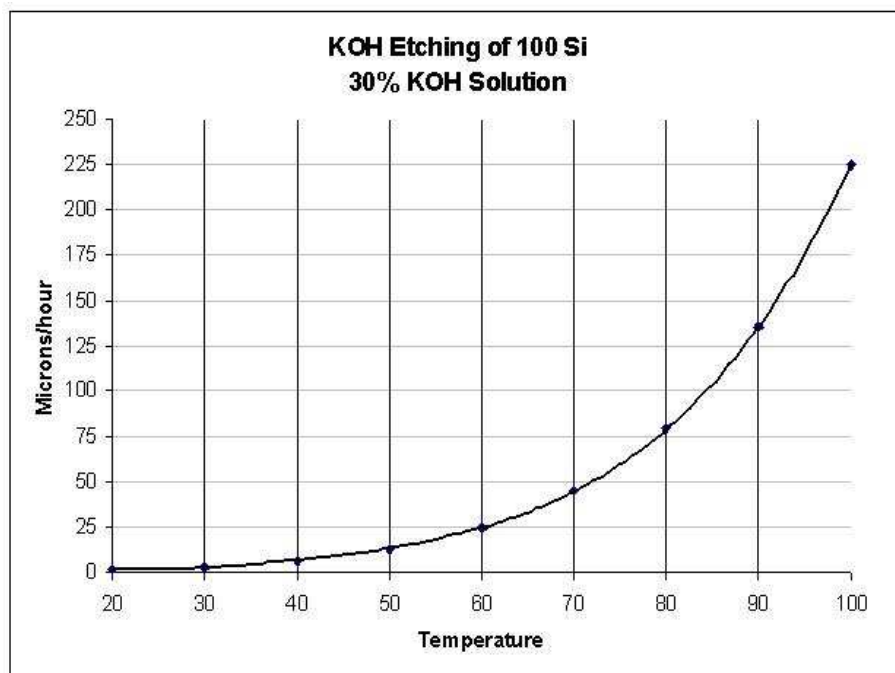
Figure 2.3 The dependence of etching rate of the [100] silicon in 30 wt.% KOH on temperature [25]
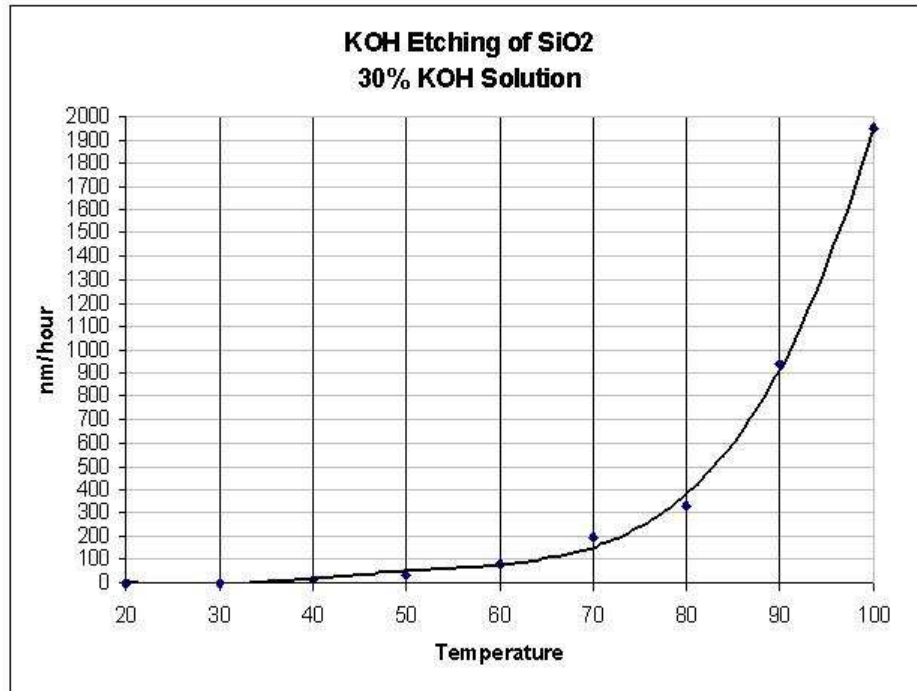
Figure 2.4 The dependence of etching rate of the silicon dioxide in 30 wt.% KOH on temperature[25]
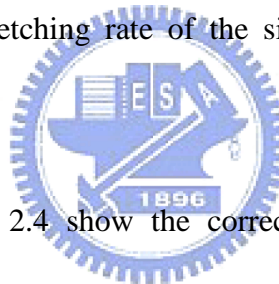
The Figure 2.3 and Figure 2.4 show the correction between the etching rate and

temperature [25]. The 30 wt.% KOH can etch amorphous silicon. We use the tape attach a part

of sample area. It immerses in the 30 wt.% KOH, until the amorphous silicon was removed.

This method leaves a well defined step profile which was measured at intervals of 25mm

along the length of the slide using a mechanical alpha step.

2.4 Conductivity Analysis

In order to investigate the conductivity of the a-Si:H, metal contacts were deposited by

thermal evaporation method onto the film. Conductivity (σ) is calculated by equation (2),

where V and I are the voltage bias and measured current. The volume of material contributing

to conductivity is determined by the width (W), length (L), and thickness (t) of a cuboid

located between the conducting contacts used to probe the sample in the Figure 2.5.

$$\sigma = \left(\frac{I}{V}\right)\left(\frac{L}{W}\right)\left(\frac{1}{t}\right) \tag{2}$$

A prepared a-Si:H film with silver contacts is show in Figure 2.5. Photo-conductivity

was measured by AM1.5G light spectrum with power at $100 mw/cm^2$. For the amorphous

silicon germanium film, the thickness is about 600 nm. For the intrinsic amorphous silicon,

the thickness is about 600 nm. The thickness of doping layer is about 200 nm .
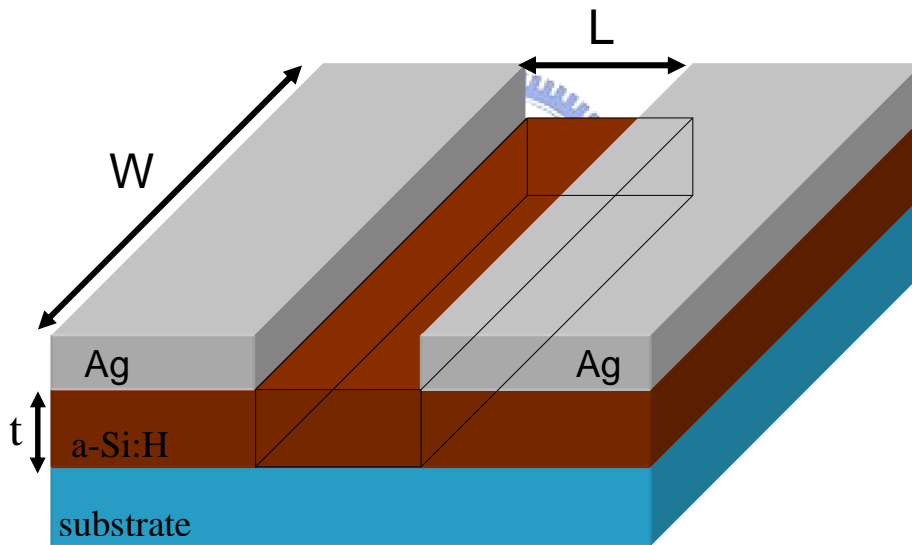
Figure 2.5   Sample configuration for the conductivity measurement of a-Si:H, where t is the film thickness

2.5 Determination of Optical Properties

2.5.1 Tauc Bandgap

The optical bandgap of thin film use UV/VIS/NIR spectrometers to measure

transmission (T) spectra were carried out between 200nm and 1.3 μm in the step of 2 nm.

Calculating optical bandgap (E_g) has to use transmission spectra and thickness of thin film in

equation (3).

$$\left(\alpha \hbar \omega\right)^{1/2} = c\left(\hbar \omega - E_{opt}\right)$$

(3)

Where α is the absorption coefficient of a-Si:H, $\hbar \omega$ is the photon energy, and E_{opt} is Tauc

optical bandgap. From Figure 2.6, $\left(\alpha \hbar \omega\right)^{1/2}$ as a function of the photo energy $\left(\hbar \omega\right)$. The

bandgap value can be determined from the expanding linear region line intercepts a-axis.
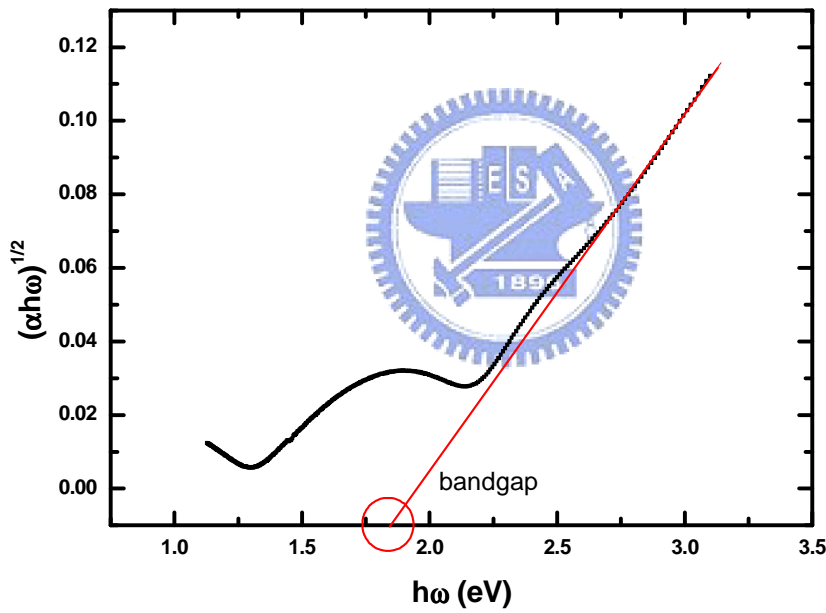
Figure 2.6 $\left(\alpha \hbar \omega\right)^{1/2}$ as a function of photon energy $\left(\hbar \omega\right)$, and the Tauc bandgap

2.5.2 Fourier Transform Infrared Spectroscopy

Since hydrogen is an important element in passivation, the incorporation and stability of

hydrogen in a-Si:H has the topic of intensive research. Infrared absorption spectroscopy is

widely use to provide information about hydrogen bonding configurations in a-Si:H [24].

Three characteristic infrared absorption bands are observed in a-Si:H: a peak at 640 cm^{-1}, and

absorption peaks in the rage of 2000-2200cm^{-1}. The peak at 640 cm^{-1} reflects the rocking

mode of hydrogen covalently bonded in all possible bonding configurations, such as silicon

monohydride (SiH), dihydride (SiH$_2$), and trihydride (SiH$_3$) and polymeric (Si-H$_2$)$_n$ bonding

configurations. Thus, this peak is used to determine the hydrogen content in a-Si:H [26]. And

peak around 2000cm^{-1} is assigned to the stretching mode of the isolated Si-H bonds and a peak

in the range of 2060-2160cm^{-1} includes contributions from the stretching mode of Si-H bonds

at internal surface, such as voids, Si-H$_2$ and Si-H$_3$.

Infrared absorption measurements were made with Fourier Transform Infrared

Spectroscopy on films deposited on crystalline silicon. The data were analyzed following

Brodksy et al. [27]. The integrated absorption, I, for each bond was determined from the

relationship.

$$I = \int \frac{\alpha(\omega)}{\omega} d\omega \tag{4}$$
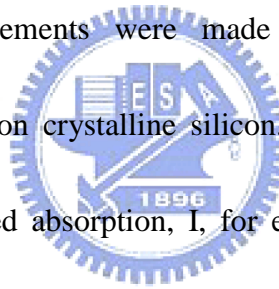
Where α(ω) is the absorption coefficient of the film at the wavenumber ω. A 'microstructure

parameter', denoted as R, is determined from the equation (5).

$$R = \frac{I_{SiH2}}{I_{SiH} + I_{SiH2}} \tag{5}$$

Where I_{SiH} and I_{SiH2} are the integrated absorption strength of the peak at wavenumber

2000 cm^{-1} and 2090 cm^{-1}, respectively. The hydrogen content C$_H$ was obtained by numerical

integration of the Si-H rocking-wagging mode [28] at 640 cm^{-1}. The complete procedure can be expressed by the following equation (6):

$$C_H(at.\%) = \frac{A_w}{N_{si}} \int_{-\infty}^{\infty} \frac{\alpha(\omega)}{\omega} d\omega \approx \frac{A_w}{N_{si}} \sum \frac{\alpha(\omega)}{\omega} \Delta\omega \qquad (6)$$

Where $A_w=1.6 \times 10^{19}$ cm^{-2} is the proportionality constant, and $N_{si}=5 \times 10^{22}$ cm^{-3} is the atomic density of pure silicon.

2.6　Measurement of Thin Film Solar Cell

An I-V characteristic is measured by performing a voltage sweep from a small reverse of forward bias whilst measuring current flow at each bias point. An illuminated I-V characteristic provides a figure for cell efficiency and incident light source is AM 1.5G with power density 100mW/cm^2. I_{sc} and V_{oc} can be determined directly from the vertical and horizontal intercepts of the sweep.

From Figure 2.7, it shows a typical illuminated I-V characteristic using real measured data. The current density is that measured current divided by cell area. The corresponding power function is shown alongside it and this is created by multiplying every voltage bias point of the I-V characteristic by the current measured at that bias. Important labeled features of the graphs include V_{oc}, J_{sc}, the bottom of the graph is maximum power density ($P_{max}=J_m V_m$).
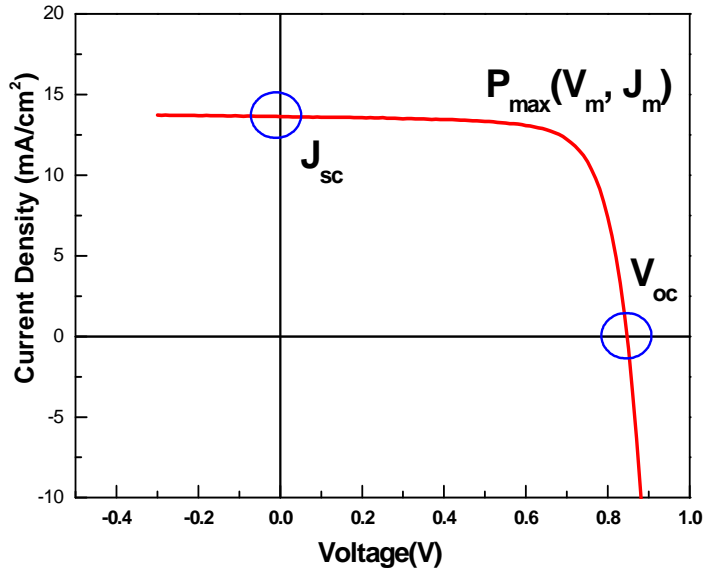
(a)
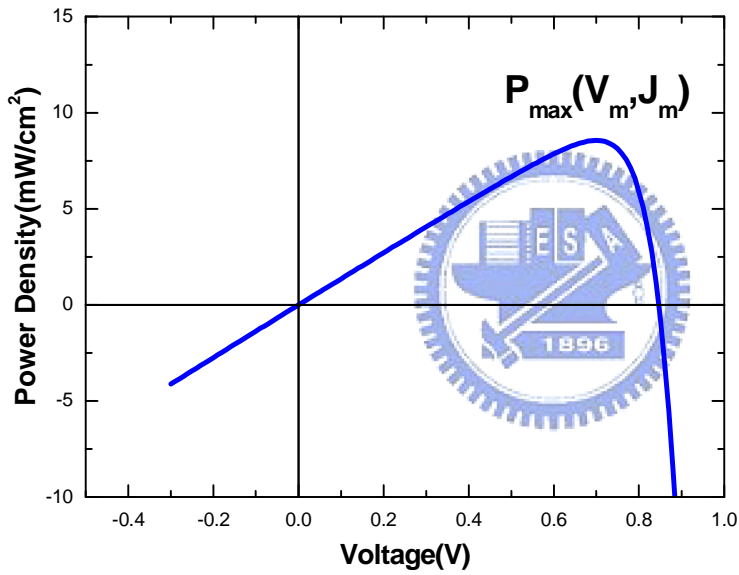
(b)

Figure 2.7   (a) The I-V characteristics and (b) power density versus voltage of solar cell, V_m and I_m are the voltage and current corresponding to the maximum power density of the cell

The solar cell efficiency (η) is the ratio between incident light power density (P_{in}) and the device convert the maximum power density. Equation (7) can calculate the cell efficiency.

$$\eta = \frac{P_{Max}}{P_{in}} = \frac{V_m I_m}{P_{in}} \tag{7}$$

Where the ratio of the maximum power density ($P_{Max} = V_m J_m$) and P_{in} is the light source

power density. And the other parameter is the fill factor (FF) can describe PV solar cell quality.

It is the ratio of the maximum power density ($P_{Max} = V_m J_m$) and a cell should supply if it was

ideal ($P = V_{oc} J_{sc}$) like equation (8). And the FF can be connect with the efficiency, it like the

equation (9).

$$FF = \frac{P_{Max}}{V_{oc} J_{sc}} \tag{8}$$

$$\eta = \frac{V_m I_m}{P_{in}} = \frac{V_{oc} J_{sc} FF}{P_{in}} \tag{9}$$

Chapter 3   Result and Discussion

3.1   Optimization of Intrinsic Hydrogenated Amorphous Silicon

3.1.1   Effect of the Silane Flow Rate on the Film Property

The optoelectronic properties of the a-Si:H deposited by the PECVD are dominated by deposition parameters , such as pressure of the gas, flow rate , substrate temperature , power density, the electrode spacing, etc. In this work, we discuss the effects of the silane flow rate and electrode distance on the qualities of amorphous silicon thin films.

Here, the substrate temperature was held at 190°C. As shown in Figure 3.1, the dark-conductivity (σ_{dark}) and photo-conductivity (σ_{photo}) as a function of the silane flow rate are demonstrated.
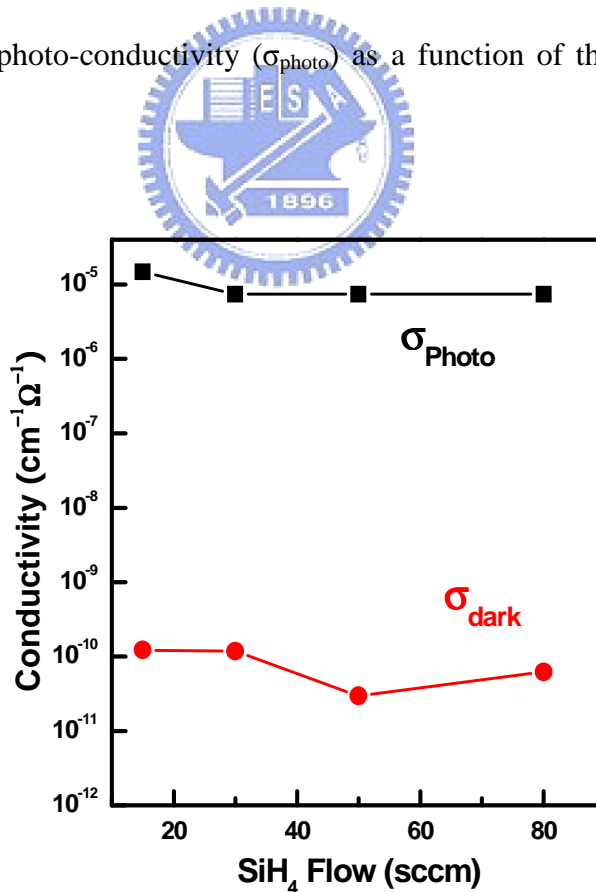
Figure 3.1   The dark-conductivity (σ_{dark}) and the photo-conductivity (σ_{photo}) as a function of the silane flow rate

From Figure 3.2, the dependence of deposition rate with on silane flow is also illustrated. The deposition rate significantly increased with raising silane flow rate from 15 to 30 sccm. When silane flow rate was raised from 30sccm to 80 sccm, the deposition rate didn't change too much. The surface reaction caused the restriction of deposition rate. Both the σ_{photo} and σ_{dark} decreased with increasing of the silane flow rate.
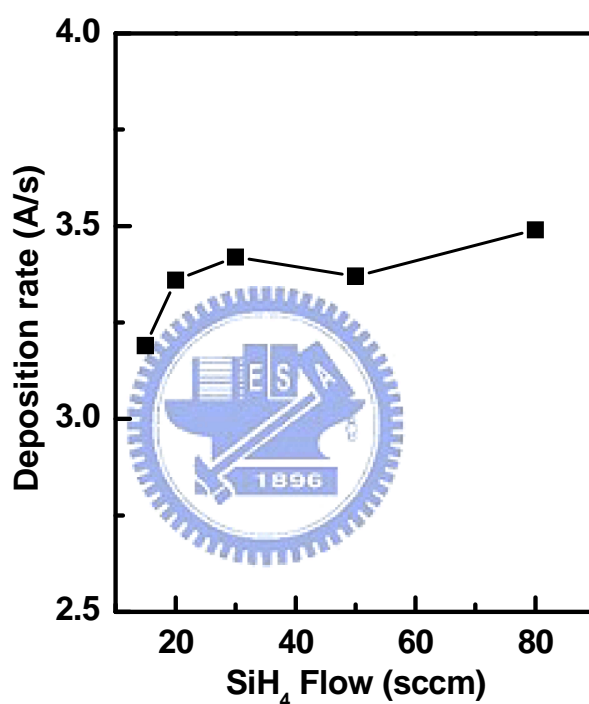
Figure 3.2   The dependence of deposition rate on silane flow rate

The dependence of hydrogen bonding configuration on silane flow rate is illustrated in the Figure 3.3. The integrated absorption of SiH and SiH_2 species depended on the silane flow rate, as shown in Figure 3.4. The hydrogen content almost was constant. When the silane flow rate varied from 30sccm to 50sccm, the R value was minimized. The silane was depleted when flow rate was less than 30sccm. Therefore, the SiH_2 bonding increased in the Figure 3.4.
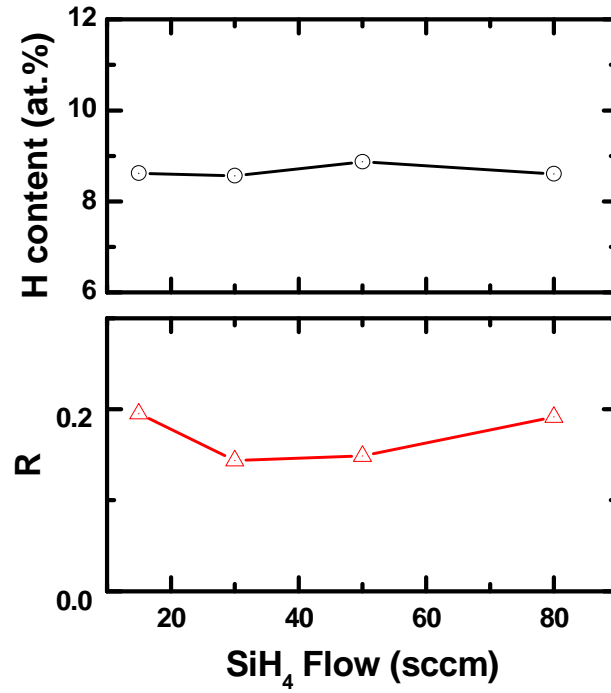
Figure 3.3 The microstructure parameters and the hydrogen content as a function of the silane flow rate
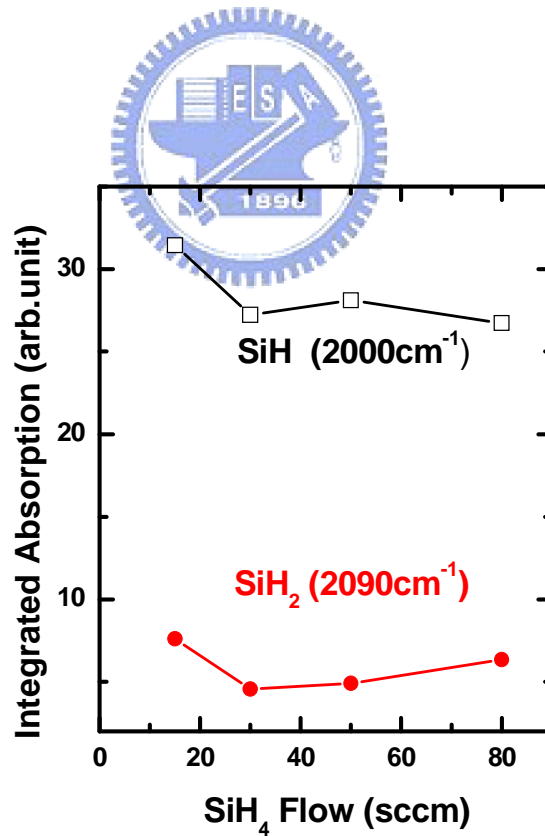
Figure 3.4 The integrated absorption of the SiH and SiH$_2$ bonding configurations as a function of the silane flow rate

On the contrary, the silane flow rate was so much that induced gas phase reaction

drastically. The SiH$_2$ bonding increased slowly as silane flow rate from 50sccm to 80 sccm.

The good qualities of amorphous silicon thin films were attained while the silane flow rate

varied from 30 sccm to 50 sccm. The films contained a majority of SiH$_2$ bonding while the

silane entirely decomposed, which was in agreement with the study of Knights and Lujan [29]

and Street et al. [30].

3.1.2   Effect of the Electrode Spacing on the Film Property

The photo- and dark-conductivity of intrinsic a-Si:H was depended on electron spacing,

as shown in the Figure 3.5. The dark-conductivity decreased with increasing electrode
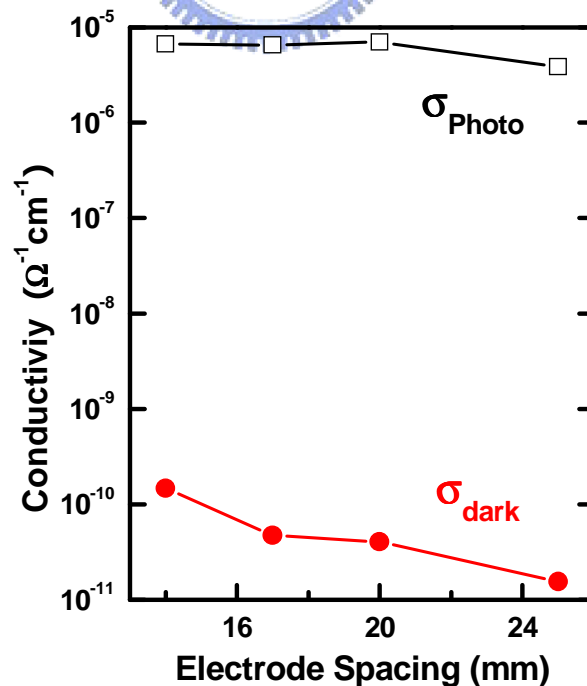
spacing.

Figure 3.5   Dependence of photo- (σ_{photo}) and dark-conductivity (σ_{dark}) of intrinsic a-Si:H on the electrode spacing

Due to the property of defect would cause the film to be more conductive or resistive, the quality of films didn't determine by the dark-conductivity. From the Figure 3.6, deposition rate significantly increased as raising electrode spacing. Increasing electrode spacing induced more gas-phase reaction. That is reason the deposition rate increase strongly when the electron spacing varied from 20mm to 25mm.
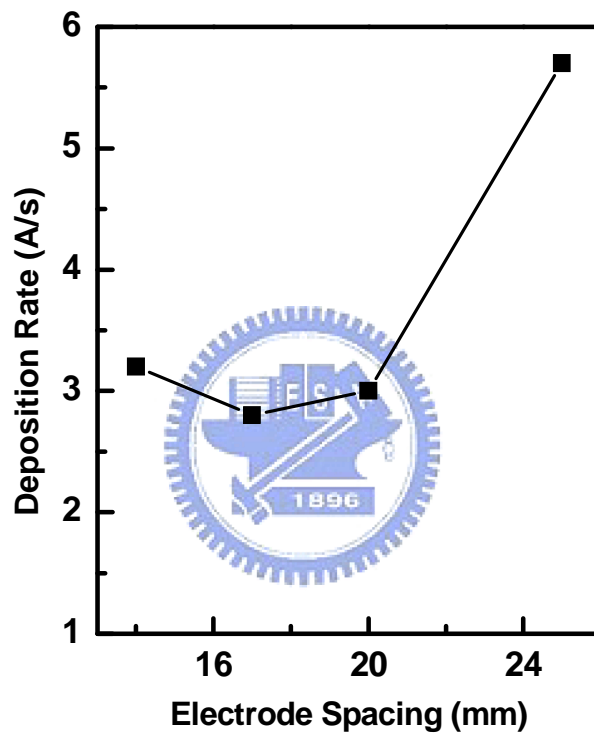
Figure 3.6   The deposition rate as a function of the electrode spacing

The results of IR spectra were shown in the Figure 3.7, including the hydrogen content and microstructure parameters with different electrode spacing, respectively. From the Figure 3.8, the hydrogen bond configuration of SiH and SiH_2 bonding was as a function of the electrode spacing.
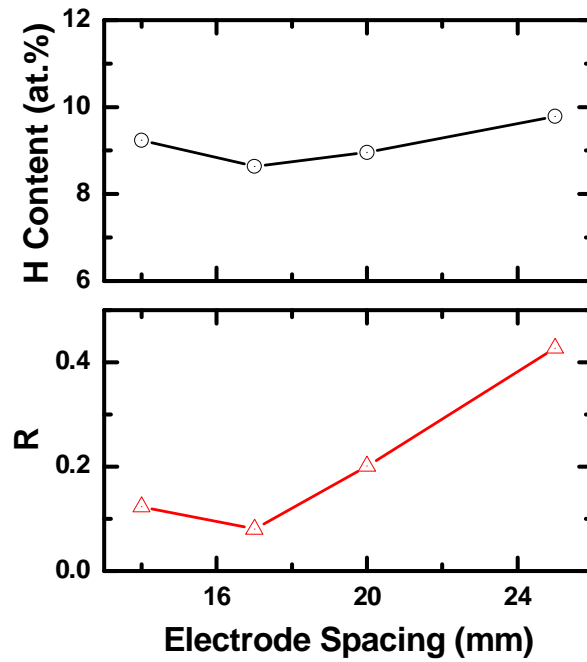
Figure 3.7 The hydrogen content and microstructure parameters versus the electrode distance, respectively
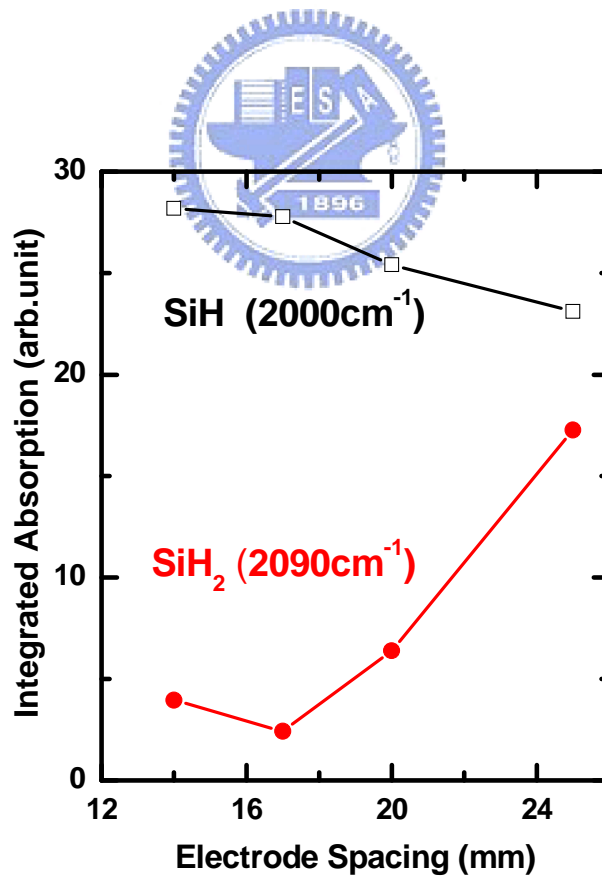
Figure 3.8 The integrated absorption of the SiH and SiH$_2$ bonding configurations versus the electrode spacing

It figured out that the increases of microstructure and hydrogen content were due to increase electrode spacing. The electrode spacing significantly affected on SiH and SiH_2 species contained in the film. When the electrode distance increased, it caused more gas-phase reaction. Therefore, it induced the increase of SiH_2 bonding. It concluded the optimal electrode spacing of film quality was in the range of from 14mm to 17mm.

The different hydrogen bonding configuration within the film can be understood from Paschen's law. Increasing pressure or electrode spacing, the electrons are more likely to collide with the plasma constituents than the electrodes. Thus, it promotes polymerization and can lead to the inclusion of SiH_2 chain within the film. On the other hand, as pressure is lowered or as electrode spacing is decreased, the electron energy is limit by collision with the electrodes. In this study, it concluded that increasing electrode spacing induces more gas-phase reaction.
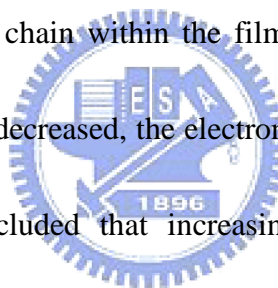
3.2 Doping of Hydrogenated Amorphous Silicon

3.2.1 Phosphorus Doping of n-type a-Si:H

The purpose of doping is to change electrical conductivity and its magnitude by adding a controlled amount of impurity atoms. The principal doping elements used in a-Si:H are the same as in crystalline silicon, boron for p-type and phosphorus for n-type material. It change conductivity of a-Si:H by mixing the silicon source gas, silane (SiH_4), with phosphine (PH_3) or diborane (B_2H_6) during deposition using the glow discharge method [31].
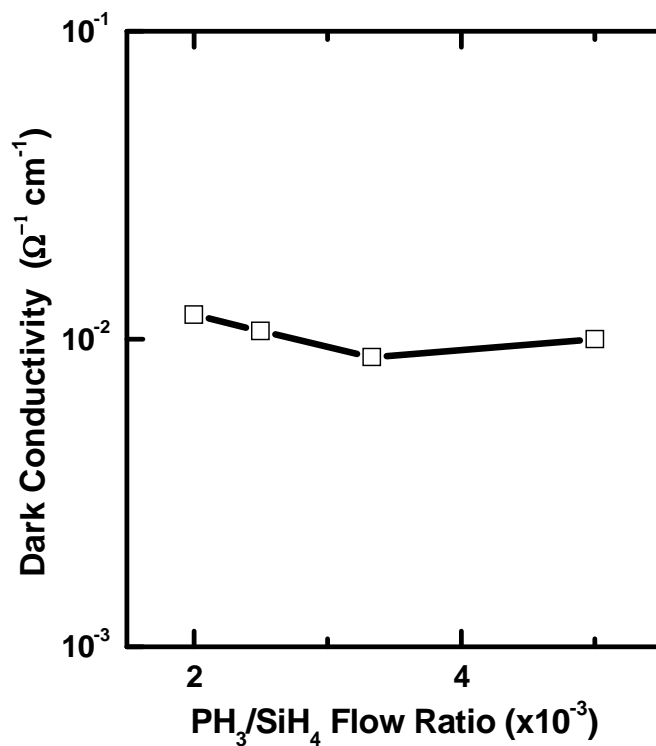
Figure 3.9 Dark-conductivity as function of the phosphine-to-silane flow ratio
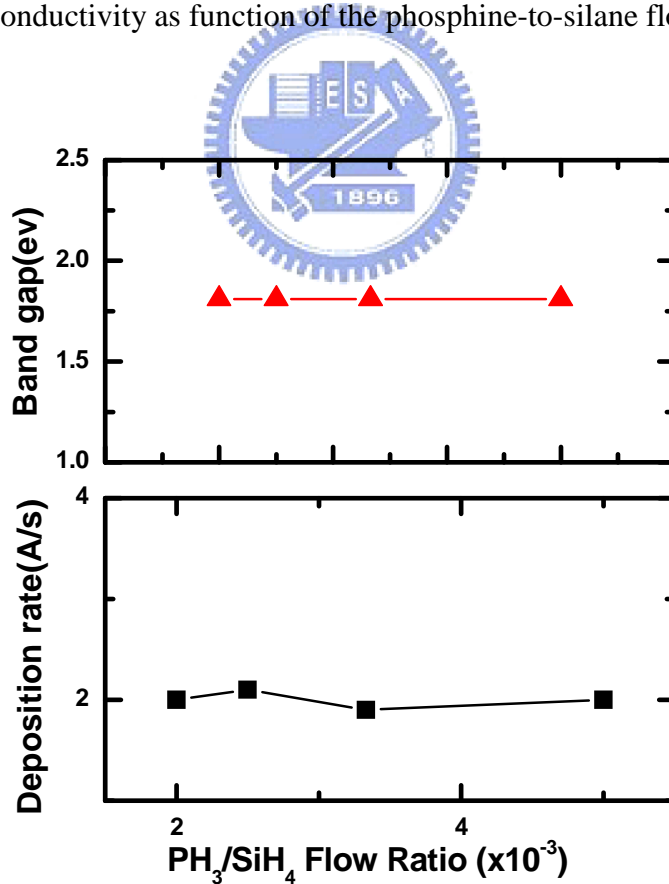
Figure 3.10 The bandgap and deposition rate as function of the silane-to-phosphine flow ratio

From the Figure 3.9, the dark-conductivity as a function of the diborane-to-silane flow ratio. As a result of heavy doping, the dark-conductivity didn't change too much. The dark-conductivity was almost 10^{-2} ($\Omega^{-1}Cm^{-1}$). As shown in the Figure 3.10, the bandgap and deposition rate as a function of phosphine-to-silane flow ratio. The doping material was too small concentration to change the bandgap.

3.2.2   Boron Doping of p-type a-Si:H

The dark-conductivity (σ_d) of p-type a-Si:H as a function of the diborane-to-silane flow ratio, as shown in the Figure 3.11. The conductivity increased as increasing flow ratio. But the diborane-to-silane flow ratio was large than 1, the conductivity didn't increase. Because the doping of a-Si:H inevitably caused the creation of dangling bond [32], it reduced the conductivity.
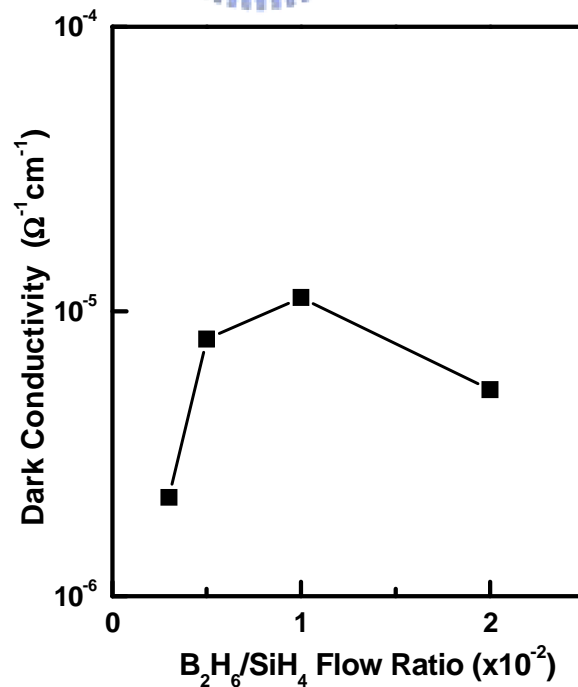
Figure 3.11   The dark-conductivity of the p-type a-Si:H as a function of the diborane–to-silane flow ratio

An additional important different between a-Si:H and single crystal silicon is that when the concentration of boron and phosphorous atoms in a-Si:H increase, then Fermi level doesn't move close to the valence and conduction band mobility edges than 0.3eV and to 0.15eV, respectively.
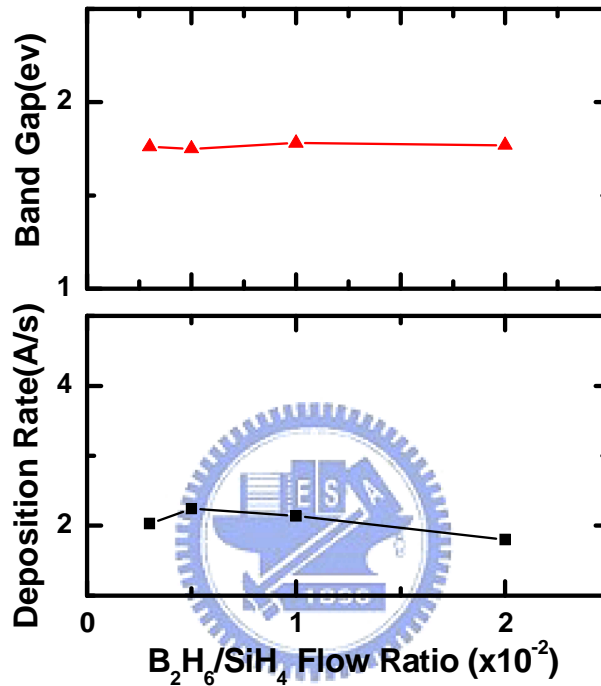
Figure 3.12   Bandgap and deposition rate versus the diborane-to-silane flow ratio

The presence of tail and defect states in the bandgap does not allow a full shift of the Fermi level towards the band edges. This is the reason the conductivity of p-type amorphous silicon was lower than n-type.

3.3   Optimization of Hydrogenated Amorphous Silicon Carbide

The purpose of alloying a-Si:H for photovoltaic application is to shift the optical absorption spectrum to higher of lower photon energies and in this way to adjust the optical sensitivity of a-Si:H to different parts of the solar spectrum. The absorption of a-Si:H can be

slightly changed by varying the hydrogen content in a film [33]. This is done by changing the

deposition conditions, such as the substrate temperature of dilution of silane with hydrogen. A

substantial shift of the absorption coefficient can be achieved by alloying a-Si:H with carbon,

oxygen, nitrogen or germanium.
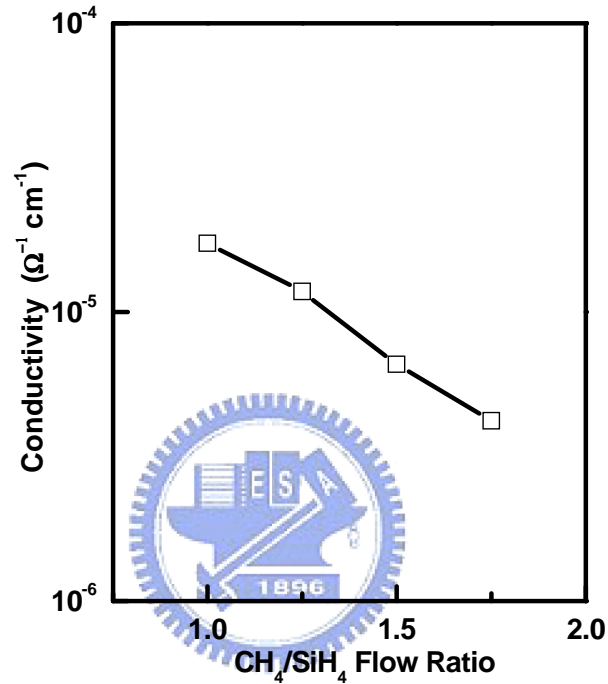
Figure 3.13   The conductivity of a-SiC:H versus the methane-to-silane flow ratio

Alloying can easily be accomplished by adding the appropriate gases to the silane

source gas in the CVD process. Amorphous silicon carbide is mixed silane with methane in

the process. It can easily change the amorphous silicon bandgap by varying the methane-to-

silane flow rate ratio [34, 35]. The conductivity and bandgap depended on methane-to-silane

flow ratio, as shown in the Figure 3.13. The conductivity of doped a-SiC:H decreased strongly,

when the methane-to-silane flow ratio increased. Because the defect of a-SiC:H was induced

more by alloying carbon.
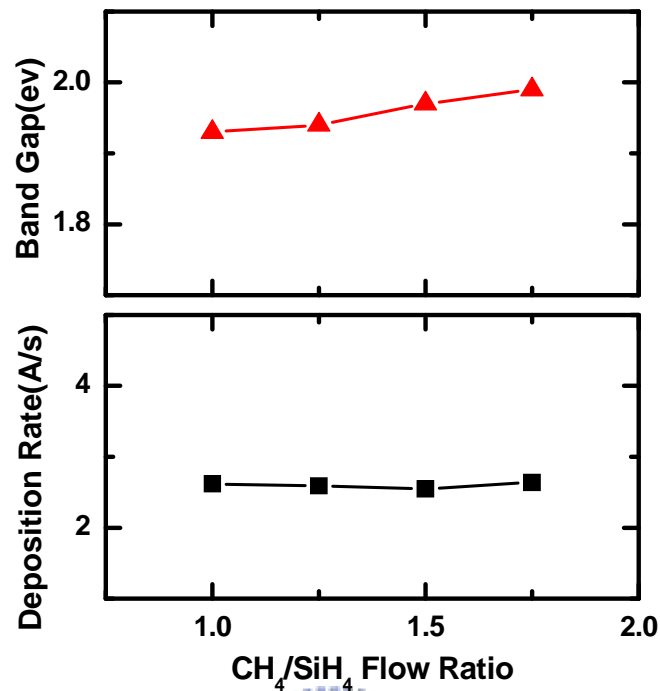
Figure 3.14   The bandgap and deposition rate as a function of the methane-to-silane flow ratio

The bandgap verses methane-to-silane flow ratio as shown in the Figure 3.14. The effective of alloying carbide can improve bandgap for amorphous silicon. The bandgap of the p-type amorphous silicon typical is 1.7 eV, but the amorphous silicon carbide was large than 2 eV. Therefore, amorphous silicon carbide can improve the device performance by inducing more photo energy to the device. On the other hand, alloying carbon would reduce the conductivity. Thus, The p-layer a-SiC:H is a trade-off between conductivity and bandgap.

3.4 Hydrogenated Amorphous Silicon Solar Cell

3.4.1 Solar Cell Fabrication on TCO-Coated Glass

In a-Si:H, the diffusion length of the charge carriers is shorter than in crystalline silicon.

In intrinsic a-Si:H, the ambipolar diffusion length is about 0.1 to 0.3 μm. In doped a-Si:H layers,

the defect density of doping a-Si:H is two or three orders of magnitude higher than intrinsic

a-Si:H. Due to the short diffusion length the photogenerated carriers would virtually all

recombine in the doped a-Si:H layers before reaching the depletion region of the p-n junction.

Therefore, an a-Si:H solar cell is designed differently compared to the standard p-n junction of

a crystalline silicon solar cell.

The doped layer are usually very thin at a-Si:H thin film solar cell. The thickness of

p-type a-SiC:H layer is less than 30nm thick, the thickness of the a-Si:H p-layer is less than

30nm thick, and an n-type a-Si:H is less than 30nm thick. The doping layer has two function of

the amorphous silicon solar cell. First, a sufficiently high electrical conductivity is required for

both p- and n- layers in order to form a high built-in voltage across the p-i-n junction. Second,

the doping layers establish low loss ohmic electrical contact with the electrode. The

steabler-Wronski effect deteriorate the collection of carriers, the thickness of intrinsic

amorphous silicon can't be too thick. So the optimal thickness of the thickness of the intrinsic

layer is in the range of 250nm to 320 nm [36]. The deposition conditions of each layer in the

fabricated a-Si:H solar cell are listed in the Table 3.1.

	p-layer (a-Si:H)	p-layer (p-a-SiC:H)	i-layer (i-a-Si:H)	n-layer (n-a-Si:H)
Substrate temperature (℃)	190	190	190	190
Deposited material	$SiH_4+B_2H_6$	$SiH_4+CH_4+B_2H_6$	SiH_4	$SiH_4+PH_3+H_2$

Table 3.1 The deposition condition of each layer in the fabricated a-Si:H solar cell
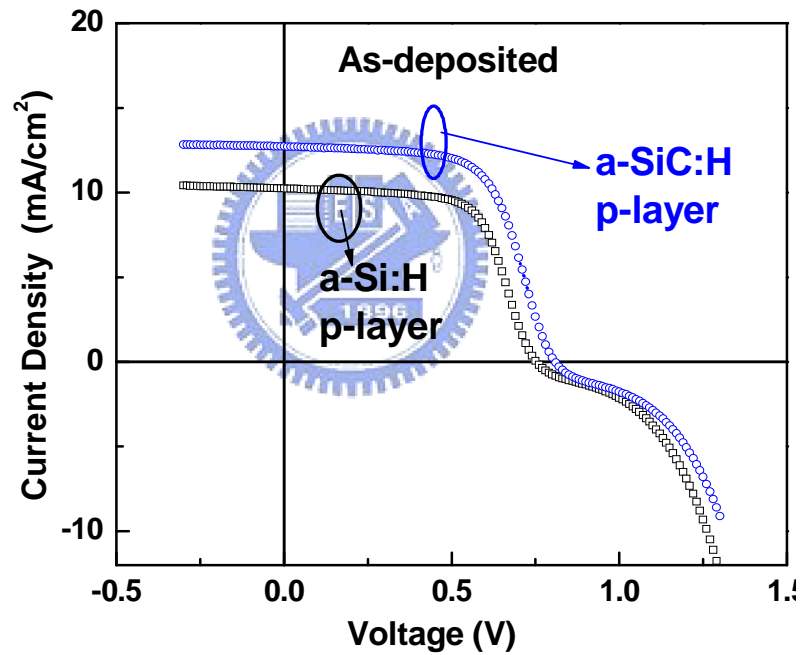
Figure 3.15 Photovoltaic performance of the as-deposited solar cell with a-Si:H and a-SiC:H as window layers

From the Figure 3.15, photovoltaic performances of the as-deposited solar cell with

a-Si:H p-layer and a-SiC:H p-layer, respectively. The characteristic of solar cell with different

p-layer material listed in Table 3.2. The cell with a-SiC:H p-layer and buffer layer (a-SiC:H)

shows increase in the open-circuit voltage (V_{oc}) from 0.75V to 0.78V and in the short–circuit

current (J_{sc}) from 10.23 mA/cm^2 to 12.76 mA/cm^2 at the same time. Because the wide bandgap

p-layer also increases the open-circuit voltage by reducing recombination at the p-i interface

[37].

p-layer	V_{oc}(V)	J_{sc}(mA/cm2)	FF(%)	η(%)
a-Si:H (1.75eV)	0.752	10.23	65	5
a-SiC:H (1.94eV)	0.788	12.76	64.12	6.57

Table 3.2   The solar cell parameters with different p-layer material
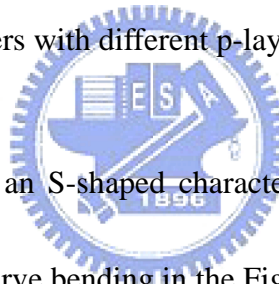
But in the I-V curve shows an S-shaped character, which the current starts falling off

already at low forward bias. The curve bending in the Figure 3.15 has shown an imperfection of

the cell. Therefore we performed a thermal annealing process try to eliminate the current

instability and enhance the performance of the solar cell.

3.4.2   Effect of Annealing on cell Performance

In the Figure 3.15 shows an S-shaped character, which the current starts to fall off already

at low forward bias. In order to find the origin for this S-shaped I-V characteristic, the

photovoltaic property of a pin type solar cell is characterized by the series resistance R_s and the

shunt resistance R_{sh}. Base on the previous study the bias-annealing treatment is expected to

increase the ionized dopant concentration of the contact layers and thereby improve cell

performance. The bias-annealing increased the open-circuit voltage, fill factor, and the cell efficiency [38]. Their conclusion is the series resistance and the shunt resistance of the hydrogenated amorphous silicon solar cell can be observed to decrease and increase respectively after bias-annealing [39].
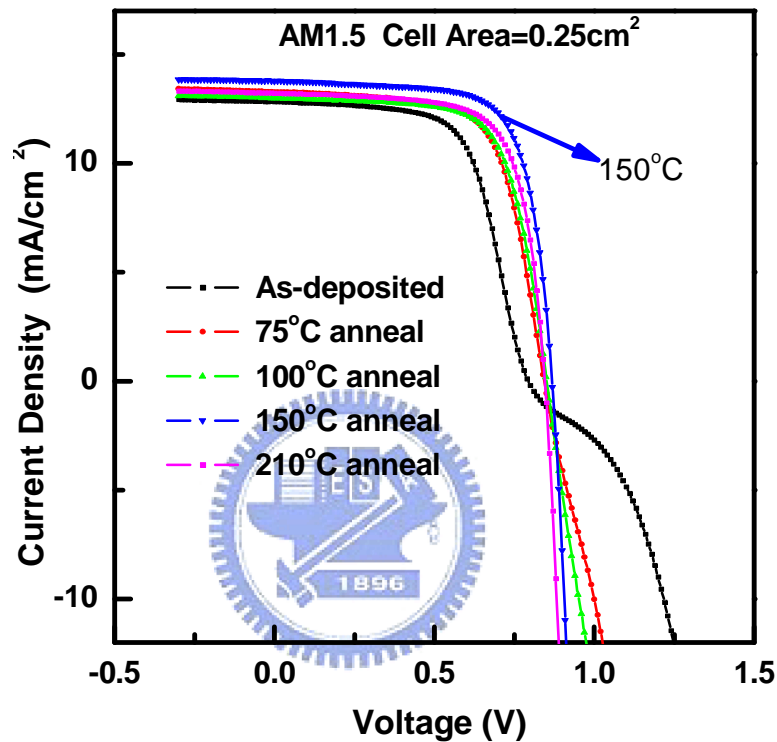
Figure 3.16   The I-V curves for the as-deposited, and the annealed solar cell after annealing at 75℃, 100℃, 150℃, 210℃, respectively

The important parameter is annealing temperature. Y. Arai et al. eliminated the process of bias-annealing. They also can improve solar cell performance by annealing without bias [40]. Figure 3.16 shows the I-V curve for the as-deposited, and the annealed solar cell after annealing temperature at 75℃, 100℃, 150℃, 210℃, respectively. The result shows that with adequate annealing temperature the cell performance can be improved greatly, which can be seen in the

Figure 3.17. The results in the Figure 3.17 indicate significant increase of V_{oc} and FF, while J_{sc}

remains the same.
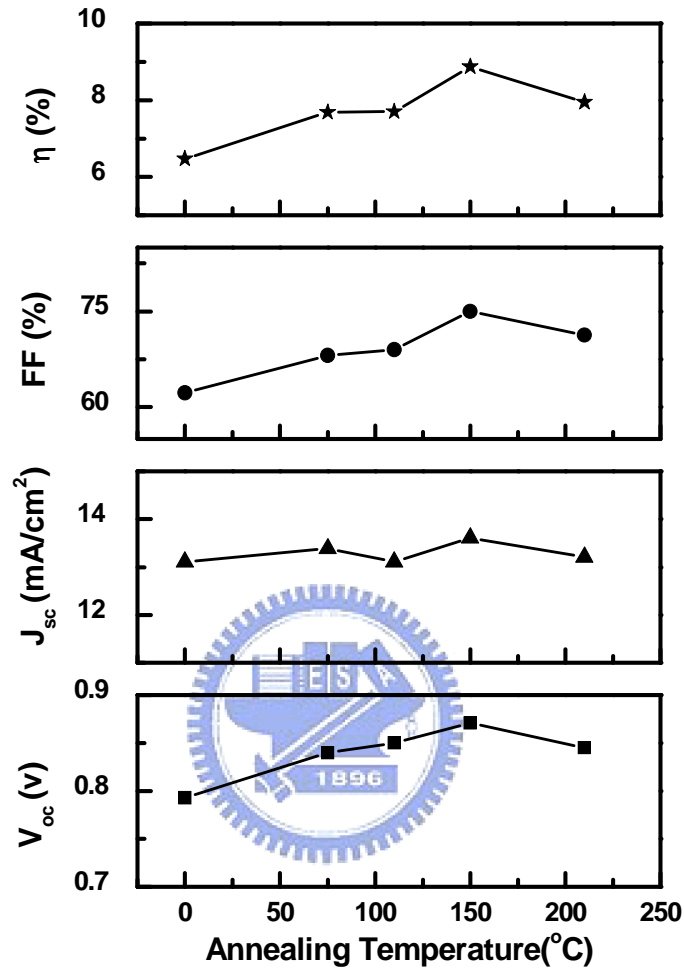
Figure 3.17 V_{oc}, J_{sc}, fill factor and efficiency of the solar cell as a function of the annealing
temperature

In the thin film silicon solar cell, there are three main factors can affect the fill factor.

First, the recombination loss in the i-layer or at the p/i and n/i interface. Second, partial

micro-shunts through the i-layer. Third, the contact and doped layers are too high resistance

[41]. The open-circuit voltage is main effect in the shunt resistance or the depletion region of

device. The photovoltaic performance starts to decay at the annealing temperature of 210℃

which may due to the degradation of interface quality.

In order to investigate the thermal annealing effect for the solar cell, experiment of the sequence between Ag deposition and annealing was carried out Ag deposition and annealing was carried out. The IV curve of the solar cell which were annealed before and the Ag electrode was deposited, as compared to the as-deposited cell, as shown in the Figure 3.18. The result indicates that the n/Ag interface and contact quality is main issue for the thermal annealing. The as-deposited and the annealing without Ag electrode didn't change observably. But the annealing after Ag electrode deposited improved performance with annealing 150 ℃.
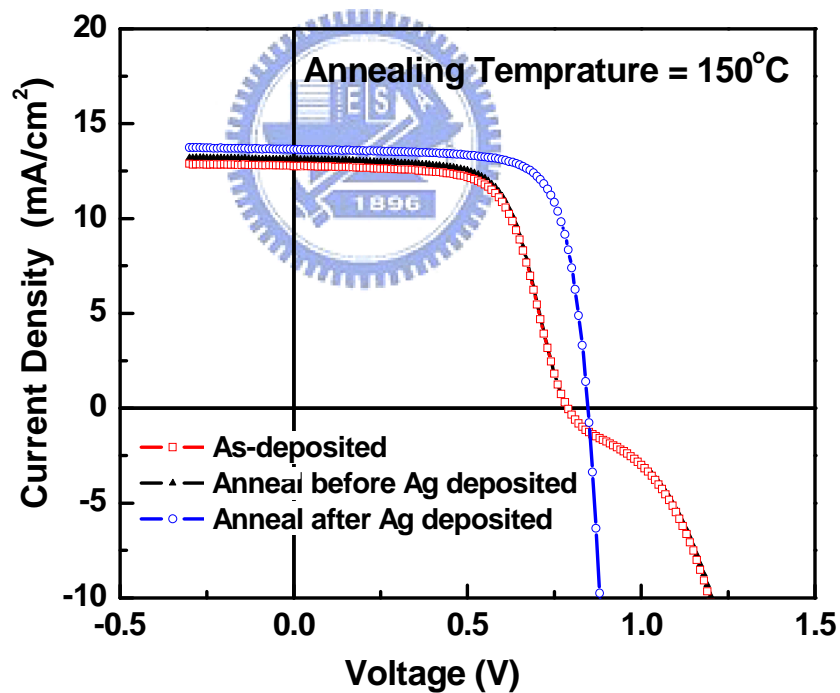
Figure 3.18   The I-V curves of the solar cells which were annealed before and after the Ag electrode was deposition, as compared to the as-deposited cell

	V_{oc}(V)	J_{sc} (mA/Cm^2)	FF (%)	η (%)
As-deposited	0.788	13.11	65.32	6.75
Annealed before Ag deposition	0.788	12.76	65.27	6.57
Annealed after Ag deposition	0.851	13.75	74.11	8.68

Table 3.3 The performance of the as-deposited solar cell and the annealed solar cell where the annealing was done before and after the silver deposition, respectively.
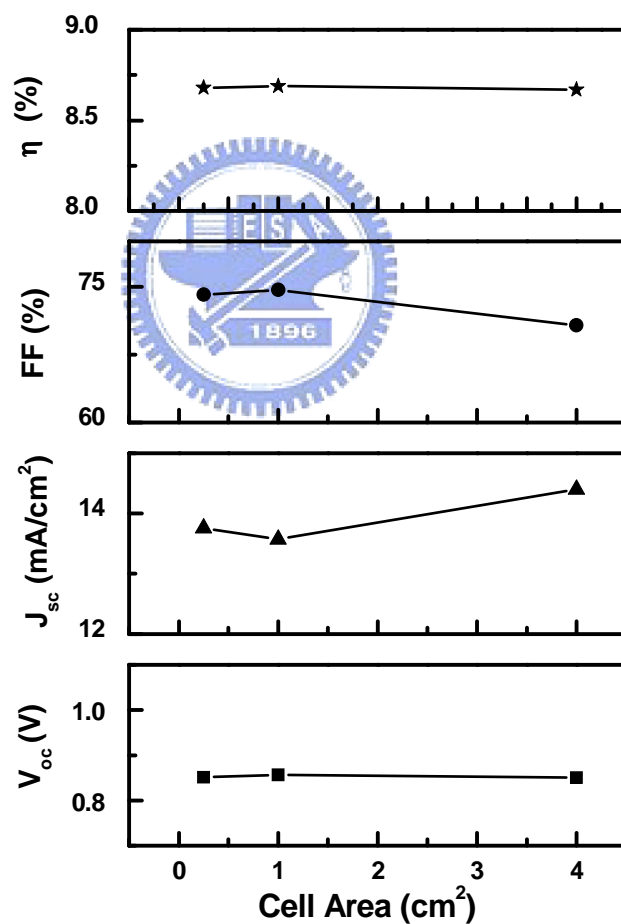
Figure 3.19 Diagrams of V_{oc}, J_{sc}, fill factor and efficiency with different solar cell area of 0.25cm^2, 1cm^2 and 4cm^2

Cell area (cm^2)	V_{oc} (V)	J_{sc} (mA/cm^2)	FF (%)	η (%)
0.5×0.5	0.85	13.75	74.11	8.68
1.0×1.0	0.85	13.57	74.66	8.69
2.0×2.0	0.85	14.4	70.75	8.67

Table 3.4   The solar-cell performance with cell area of 0.5×0.5 cm^2, 1.0×1.0 cm^2 and 2.0×2.0 cm^2

It can conclude the thermal annealing can get better between silver and n-type layer interface. Because the defect in the interface introduce states in the semiconductor bandgap which can trap charges and influence the potential distribution at the junction. A high density of interface states reduces the open-circuit voltage and degrades the photovoltaic performance of the devices. The cells with size of 0.5×0.5 cm^2, 1.0×1.0 cm^2 and 2.0×2.0 cm^2 were fabricated to verify the cell performance related to uniformity. The results can be seen in the Figure 3.19 and Table 3.9. The result shows cell performance did not degraded on the cell area was enlarged to 2.0×2.0 cm^2. The efficiency of about 8.5 % and high performance were achieved by the large area solar cell.

Chapter 4 Conclusion and Future Work

4.1 Conclusion

In this work, we have studied the property of a-Si:H as function of the silane flow rate, electrode spacing and dopant concentration. Increasing the electrode spacing promoted polymerization and can lead to the inclusion of SiH_2 chain within the film. The high quality intrinsic a-Si:H was obtain at which contains 8~9 atomic % of hydrogen predominated bonded as SiH configuration. The p-layer and n-layer have been doped with appropriate dopant concentration. Alloying a-Si:H with carbon causes the bandgap to widen, but it also reduce the conductivity. Usage of the wide bandgap p-layer would increases the open-circuit voltage and the short-circuit current of the solar cell by increasing incident light and reducing electron-hole recombination at the p-i interface. In this study, the optimal a-SiC:H window layer has bandgap 1.94ev and carbon composition 20 %.The annealing would affect solar cell performance significantly with optimal annealing temperature of 150℃. The n/Ag interface is the main improvement of the solar cell when underwent thermal annealing. The structure of a-Si:H solar cell with area sizes of $2\times2cm^2$ and $1\times1cm^2$ was also fabricated, respectively. The cell performance did not degrade on the cell area was enlarge to $2\times2cm^2$. The best conversion efficiency of 8.67% was achieved for area of $2\times2cm^2$.
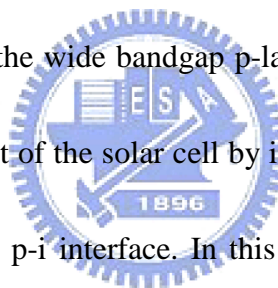
4.2 Future Work

The performances of single junction a-Si:H solar cells decrease during the initial stage of due to light induced degradation. The solar cell degradation due to illumination is the manifestation of the Staebler-Wronski effect. After the initial degradation, the performance of solar cells stabilizes. Therefore, the a-Si:H solar cell structure and the properties of the individual a-Si:H based layers must be optimized for the light soaked state. In addition, in this study we considered only single-junction solar cell. This work can be extended for tandem solar cells, with a-Si:H cell as the bottom cell and the a-SiGe or μc-Si thin film solar cell as the top cell for very high efficiency.

Reference

[1]   German Advisory Council on Global Change, "World in Transition–Towards Sustainable Energy Systems", Earthscan, London (2003)

[2]   M.A. Green, "Third Generation Photovoltaics:Ultra-High Efficiency at Low Cost", Springer-Verlag, Berlin, (2003)

[3]   D.L. Staebler and C.R. Wronski, "*Reversible conductivity changes in discharge–produced amorphous Si*", Appl. Phys. Lett., **31**, 292 (1977)

[4]   D.E. Carlson, R.R. Arya, M. Bennet, L.F. Chen, K. Jansen, Y.M. Li, J. Newton, K. Rajan, R. Romero, D. Talenti, E. Twesme, F. Willing and L. Yan, "*Commercialization of multi -junction amorphous silicon modules*", Proc. 25th IEEE Photovolt. Specialists Conf., 1023 (1996)

[5]   S. Guha, "*Amorphous silicon alloy solar cells and modules-opportunities and challenges*", Proc. 25th IEEE Photovolt. Specialists Conf., 1017 (1996)

[6]   S. Fujikake, K. Tabuchi, A. Takano, T. Wada, S. Saito, H. Sato, T. Yoshida, Y. Ichikawa and H. Sakai, "*Film-substrate a-Si solar cells and their novel process technologie*s", Proc. 25th IEEE Photovolt. Specialists Conf., 1045 (1996)

[7]   G. Hagedorn, "*Hidden energy in solar cells and photovoltaic power station*s", Proc. 9th Europ. Photovolt. Solar Energy Conf., 542 (1989)

[8]   J. M. Woodcock, H. Schade, H.Maurus, B. Dimmler, J. Springer and A. Ricaud, "*A study of the upscaling of thin film solar cell manufacture towards 500 MWp per annum*", Proc. 14th Europ. Photovolt. Solar Energy Conf., 857 (1997)

[9]   D.E. Carlson and C.R. Wronski, "*Amorphous Si solar cell*", Appl. Phys. Lett., **28**, 671 (1976)

[10] H. Sakai and Y. Ichikawa, "*Process technology for a-Si/A-Si double stacked tandem solar cells with stabilized 10% efficiency*", J. Non-Cryst. Solids, **137**, 1155 (1991)

[11] G. Nakamura, K. Sato and Y. Yukimoto, "*High performance tandem type amorphous solar cells*", Proc. 16th IEEE Photovolt. Specialists Conf., 1331 (1982)

[12] J. Yang, A. Banerjee and S. Guha, "*Triple-junction amorphous silicon alloy solar cell with 14.6% initial and 13.0% stable conversion efficiencies*", Appl. Phys. Lett., **70**, 2975 (1997)

[13] Y. Tawada, H. Okamoto and Y. Hamakawa, "*a-SiC:H/a-Si:H heterojunction solar cell having more than 7.1% conversion efficiency*", Appl. Phys. Lett., **39**, 237 (1981)

[14] G. Nakamura, K. Sato, Y. Yukimoto, K. Shirahata, T. Murahashi and K. Fujiwara, "*Amorphous SiGe:H for high performance solar cells*", Jap. J. Appl. Phys., **20,** 291 (1981)

[15] H.W. Deckman, C.R. Wronski, H. Witzke and E. Yablonovitch, "*Optically enhanced amorphous silicon solar cells*", Appl. Phys. Lett., **42**, 968 (1983)

[16] S. Guha, K.L. Narasimhan, S.M. Pietruszko, "*On light-induced effect in amorphous hydrogenated silicon*", J. Appl. Phys., **52**, 859 (1981)

[17] A. Matsuda, T. Yamaoka, S.Wolff, M. Koyama, Y. Imanishi, H. Kataoka, H. Matsuura and K. Tanaka, "*Preparation of highly photosensitive hydrogenated amorphous Si-C alloys from a glow-discharge plasma*", J. Appl. Phys., **60**, 4025 (1986)

[18] A. Matsuda and K. Tanaka, "*Guiding principle for preparing highly photosensitive Si-based amorphous alloys*", J. Non-Cryst. Solids, **97**, 1367 (1987)

[19] J. Meier, S. Dubail, R. Platz, P. Torres, U. Kroll, J.A. Anna Selvan, N. Pellaton Vaucher, Ch. Hof, D. Fischer, H. Keppner, R. Flückiger, A. Shah, V. Shklover and K.D. Ufert, "*Towards high-efficiency thin-film silicon solar cells with the " micromorph " concept*", Sol. En. Mat. and Sol. Cells, **49**, 35 (1997)

[20] J. Meier, U. Kroll, S. Dubail, S. Golay, S. Fay and J. Dubail, "*Efficiency enhancement of amorphous silicon p-i-n solar cells by LP-CVD Zn*O**",** Proceedings of the 28th IEEE Photovoltaic Specialist Conference, 746 (2000)

[21] A.V. Shah, M. Vanecek, J. Meier, F. Meillaud, J.Guillet, K. Fischer, C.Droz, X. Niquille, S. Tay, E. Vallat-Sauvain, V. Terrazzoni-Saudrix and J. Bailat, "*Absorption loss at nanorough silver back reflector of thin-film silicon solar cell*s", J. Non-Cryst. Solids, **388**, 639 (2004)

[22] J. Perrin, O. Leroy and M.C. Bordage, "*Cross-Sections, Rate Constants and Transport Coefficients in Silane Plasma Chemistry*", Contrib. Plasma Phys., **36**, 3 (1996)

[23] A. Matsuda, K. Nomoto, Y. Takeuchi, A. Suzuki, A. Yuuki and J. Perrin, "*Temperature dependence of the sticking and loss probabilities of silyl radicals on hydrogenated amorphous silicon*", Surf. Sci., **227,** 50 (1990)

[24] R.A. Street, "Hydrogenated Amorphous Silicon", Cambridge University Press, Cambridge (1991)

[25] H. Seidel, L. Csepregi, A. Heuberger, H. Baumgartel, "*Anisotropic etching of crystalline silicon in alkaline solutions*", J. Electrochem. Soc., **137**, 3612 (1990)

[26] R.E.I. Schropp, M. Zeman, "Amorphous and Microcrystalline Silicon Solar Cells", Kluwer Academic publishers, Boston, p.47(1998)

[27] M.H. Brodksy, M. Cardona and J.J. Cuomo, "*Infrared and Raman spectra of the silicon-hydrogen bonds in amorphous silicon prepared by glow discharge and sputtering*", Phys. Rev., B**16**, 3556 (1977)

[28] H. Shanks, C.J. Fang, L. Ley, M. Cardona, F.J. Demond, and S. Kalbitzer, "*Infared spectrum and structure of hydrogenated amorphous silico*n", Phys. Status Solidi, B**110**, 43 (1980)

[29] J. Knights and R.A. Lujan, " *Microstructure of plasma-deposited a-Si:H film*s**",** Appl. Phys .Lett., **35**, 244 (1979)

[30] R.A. Street, J.C. Knights, and D.K. Biegelsen, "*Luminescence studies of plasma-deposited hydrogenated silicon*", Phys. Rev., B**19**, 3027 (1978)

[31] W.E. Spear and P. Le Comber, "*Substitutional doping of amorphous silicon*", Solid State Electron., **8**, 653 (1965)

[32] R.A. Street, "*Doping and the Fermi Energy in Amorphous Silicon*", Phys. Rev. Lett., **49**,1187 (1982)

[33] T. Hanma, H. Okamoto, Y. Hamakawa and T. Mastsubara, "*Hydrogen content dependence of the optical energy gap in a-Si:H* ", J. Non-Cryst. Solids, **59**, 333 (1983)

[34] D.A. Anderson and W.E. Spear, *"Photoconductivity and recombination in doped amorphous silicon"*, Phil. Mag., **35**, 1 (1977)

[35] Y. Catherine, G. Turban, and B. Grolleau, *"Reaction mechanisms in plasma deposition of Si_xC_{1-x}:H films "*, Thin Solid Films, **76**, 23 (1981)

[36] M. Kondo, K. Hayashi, H. Nishio, S. Kurata, A. Lshikawa, A. Takenaka, K. Nishimura, A.Nakajima, H. Yamagishi and K.Y. Taeada, *" Development of high efficient large area a-Si solar modules "*, Proceedings of the 13th European Photovoltaic Solar Energy Conference, Nice, 311 (1995)

[37] Y. Tawada, M. Kondo, H. Okamoto, and Y. Hamakawa, *"a-SiC:H/a-Si:H heterojunction solar cell having more than 7.5% conversion efficiency"*, Proc. 15th IEE Photovoltaic Specialists Conf., 245 (1981)

[38] G.A. Swartz, *"Reverse bias and heat treatment to improve performance of a-Si solar cells"*, Appl. Phys. Lett., **44**, 697 (1984)

[39] Tulay Serin and Necmi Serin, *"The effect of annealing on the resistance of a p/i/n structure"*, Semicond. Sci. Technol., **9**, 2097 (1994)

[40] Y. Arai, M. Ishii, H. Shinohara, and Shumpei Yamazaki, *" A single p-i-n junction amorphous-silicon solar cell with conversion efficiency of 12.65%"*, Electron Device Letters, **12,** 460 (1991)

[41] F. Meillaud, A. Shah, J. Bailat, E. Vallat-Sauvain, T. Roschek, B. Rech, D. Domine, T. Soderdtrom, M. Python and C. Ballif, *"Microcrystalline Silicon Solar Cells: Theory and Diagnostic Tools "*, Photovoltaic Energy Conversion, Conference Record of the 2006 IEEE 4th World Conference, **2**, 1572 (2006)